J. Fluid Mech. (2004), *vol.* 520, *pp.* 93–134. © 2004 Cambridge University Press
DOI: 10.1017/S0022112004001223 Printed in the United Kingdom

Weakly nonlinear cubic interactions in coastal resonance

By GUIDO M. TERRA[1,2]†, ARJEN DOELMAN[1,3], AND LEO R. M. MAAS[2]

[1]Korteweg-de Vries Institute for Mathematics, University of Amsterdam, Plantage Muidergracht 24, NL-1018 TV Amsterdam, The Netherlands

[2]Royal Netherlands Institute for Sea Research, Physics Department, P.O. Box 59, NL-1790 AB Den Burg, The Netherlands

[3]Centrum voor Wiskunde en Informatica, P.O. Box 94079, NL-1090 GB, Amsterdam, The Netherlands

(Received 29 April 2003 and in revised form 16 July 2004)

In this paper the qualitative nonlinear influence of advection and continuity on the resonance characteristics of co-oscillating coastal basins is investigated. For this purpose a weakly nonlinear analysis was carried out on the shallow-water equations describing a coastal basin resonating with exterior water-level oscillations. It extends previous work on an almost-enclosed basin with one single (Helmholtz) mode to arbitrarily shaped 'shallow' basins with an infinite number of modes. In line with that work, it is necessary to assume friction to be sufficiently weak such that it is in balance with the nonlinear effects, instead of occurring in the linearized equations. The main result of this paper is the system of Landau equations describing the slow evolution of the amplitudes of the oscillatory eigenmodes of the basin, disregarding a zero-frequency eigenmode, should it exist. The dynamics of the zero-frequency mode neglecting oscillatory eigenmodes have been discussed by others, but a consistently balanced model for small amplitudes incorporating both the zero-frequency and oscillatory modes is not yet available. The behaviour of this system, describing the dynamics of the oscillatory eigenmodes only, is analysed. On the longer time scale, it gives rise to a 'bent resonance curve', multiple equilibria (several tidal regimes under the same tidal forcing), sudden regime changes and even chaotic dynamics (when these regime changes occur in an irregular way).

1. Introduction

Tides are generated by the gravitational forces exerted by astronomical objects, mainly the sun and the moon. The direct gravitational forcing acounts for a global tidal amplitude of merely 0.27 m for the lunar and 0.13 m for the solar component (LeBlond & Mysak 1978, p. 517). In order to explain the strong tidal signal of several metres in many coastal areas, amplification due to resonance is required. A tidal basin connected to a neighbouring ocean or sea can co-oscillate with the tide at sea with increased amplitude if the basin's geometry is such that the period of one of its eigenmodes corresponds to that of the tidal motion. The amplification has been described quite well with linear theory (Defant 1961; LeBlond & Mysak 1978; Mei 1989). In this paper nonlinear corrections to this linear picture are investigated.

† Author to whom correspondence should be addressed: gmterra@science.uva.nl / terra@nioz.nl

https://doi.org/10.1017/S0022112004001223 Published online by Cambridge University Press

The nonlinear effects addressed here are due to advection and to feedback on the water depth. Besides modifying the shape of the tidal curve by generating higher harmonics, they can change the response curve (amplification as a function of forcing frequency) of the basin, which may have dramatic qualitative effects. This paper focuses on the latter effect.

Traditionally the term *coastal resonance* is used to describe the response of certain large-scale bays to forcing at one of the tidal frequencies. This response is typically classified by the nature of the response, ranging from microtidal (when the coastal tide is choked, i.e. has an amplitude less than that of the tide at open sea), via meso- to macrotidal (coastal tide moderately amplified). Yet, in its strictest sense the term is reserved to designate a so-called megatidal response, the severe amplification such as encountered e.g. in the famous Bay of Fundy (amplitudes ranging up to 8 m), Sea of Okhotsk, or near the coast of Normandy (amplitudes over 6 m). The nonlinear model for coastal resonance which we will present, is, by the approach it takes, particularly of relevance to the latter, megatidal case. It predicts that in certain circumstances the tidal response might be irregular on the longer (e.g. fortnightly) time scale.

Resonance in smaller-scale coastal basins is called *harbour resonance*. These infragravity waves (Okihiro & Guza 1995) are pronounced oscillations in near-shore sea areas and harbours with periods of a few minutes to hours, which are longer than those associated with surface wind waves, but of shorter duration than a typical tidal period. It can be considered as a special kind of coastal resonance. It is related again to an eigenmode, typical of the particular geomorphology of the area under consideration, resonating due to some forcing mechanism. In this case, the corresponding eigenfrequencies are much higher than the tidal frequencies. The importance of the more pronounced oscillations of this kind can be inferred from the fact that the phenomenon is locally often identified by a certain name: e.g. *Abiki* in Nagasaki Bay (Hibiya & Kajiura 1982), *Risagga* at Menorca (Gomis, Monserrat & Tintoré 1993) and *Marrobbio* in the Strait of Sicily (Candela *et al.* 1999). These oscillations, also called *secondary undulations* (small-amplitude, 'high'-frequency undulations accompanying the tidal, 'primary' oscillation), are perhaps less spectacular in overall appearance than megatidal oscillations, but their importance is boosted when one considers the associated currents, of importance for the flushing of the coastal areas. Observations by Golmen, Molvaer & Magnusson (1994) show that these 'perturbation' currents may in fact be of similar strength to those associated with the generating, primary tide. Several different forcing mechanisms have been put forward to explain their origin: atmospheric pressure perturbations (Hibiya & Kajiura 1982), internal wave activity (Giese & Chapman 1990), seismic activity (tsunamis), or current shear (Fabrikant 1995). This paper deals primarily with the case of coastal resonance in large-scale basins at tidal frequencies, but after a few modifications the analysis can be applied to the case of secondary undulations as well.

At present we have no knowledge of observations analysed to corroborate the behaviour described in this paper. However, most certainly there are indications that the linear picture describing the tide as a sum of harmonic tidal components is incomplete. Doodson (1924) studied the yearly variations of harmonic constants in Bombay and St. John, Bay of Fundy (see also Defant 1961, p. 309). The variation can be explained partly by long-term astronomical signals, such as the regression of the moon with a period of about 19 years, but another part is not accounted for. A similar study by Gutiérrez, Mosetti & Purga (1981), investigating year to year variability of the harmonic constants for Trieste, shows that it cannot be attributed to deficiencies of the filtering methods. Although the etymology of the word 'tides' stems from

https://doi.org/10.1017/S0022112004001223 Published online by Cambridge University Press

their periodicity, reports of irregular tides have been made throughout time. More recently, Frison *et al.* (1999) argue that, in a number of tidal areas, the astronomical constituents account for only 50–70% of water-level variability. The residual spectral contributions have often been qualified as 'noise', due to meteorological influences, river inflow and tidal interactions. Frison *et al.* (1999) analysed water-level data using new data analysis techniques that have been developed for chaotic systems. They calculate attractor dimensions and Lyapunov exponents for some tidal signals and conclude that they come from a relatively noise-free but chaotic system. Tidal predictions based on harmonic constants, describing the tidal signal as a linear sum of astronomical constituents, do not capture this. The model derived in this paper yields possible chaotic behaviour of the harmonic 'constants'. Hence it differs from the observations by Frison *et al.* (1999) who studied chaotic behaviour in the time series of water-level elevation itself instead of the amplitudes. In that sense it relates to the research of Doodson (1924) and Gutiérrez *et al.* (1981), although they considered the variability of yearly averaged results whereas the changes described in this paper would occur on a smaller time scale.

In the case of harbour resonance, reports on irregular behaviour are more common. Based on the study of surface elevations in over 50 bays adjacent to Japan, Honda *et al.* (1908) speculate that this type of coastal resonance is forced by the tide as well, for which a possible explanation is given by Fabrikant (1995). Regarding the nature of the secondary undulations these authors conclude that they

(i) vary from inconspicuous (at the Pacific coast) to conspicuous (near the Japan Sea),
(ii) vary from regular to irregular,
(iii) may often change their periods continuously,
(iv) often appear in phase with the tide,
(v) often have periods reflecting quarter-wavelength resonance,
(vi) often disappear outside the bay,
(vii) have the same period as when excited in response to a storm.

Although this does not rule out the possibility of incidental forcing by strong winds or intense atmospheric pressure disturbances, the persistence of the secondary undulations suggests an ever-present source, such as due to tidal motion in the adjacent sea. The observations of the secondary undulations accompanying the tide show that the response of a local eigenoscillation may differ in character from periodic, tidally phase-locked, to aperiodic (Nakano 1932). This indicates some kind of nonlinear coupling to the tide.

A model aimed at describing such nonlinear coupling has been developed previously by assuming the spatial structure of the response in the bay to be as simple as possible (namely spatially uniform), see Miles (1981); Green (1992); Maas (1997). Such a uniform spatial structure is a property of the so-called *Helmholtz* (or *pumping*, or breathing) mode, and requires a specific geographic setting: an almost-enclosed, deep and small basin, such that the length of the basin is much shorter than the tidal wavelength. Although this allows the nonlinear temporal response to be understood (Maas & Doelman 2002; Doelman, Koenderink & Maas 2002), the stringent requirements on the shape of the resonator render it less applicable to describe the response of the majority of (half open) bays considered by Honda *et al.* (1908). The results in the present paper form a direct generalization of Maas & Doelman (2002) and Doelman *et al.* (2002) to the case of eigenoscillations in such half-open, quarter-wavelength basins. Note that the term *quarter-wavelength* is used here to describe modes in a two-dimensional basin with non-uniform depth as well, i.e. to denote modes with spatial structure, in contrast to the Helmholtz mode.

https://doi.org/10.1017/S0022112004001223 Published online by Cambridge University Press

In line with the observations, we will assume the resonating oscillation to be nearly absent outside the bay. As will be shown here, one can derive amplitude equations that govern the evolution of the quarter-wavelength-type eigenmodes, the simplest of which is identical to the equation governing the Helmholtz mode in the more specific setting of an almost-enclosed basin. Although the terminology in this paper is adapted to the tidal case, the analysis can be applied to the infragravity regime as well. If the infragravity waves are the dominant oscillation in the basin, one only needs to change the time scale from the tidal period to the period of the harbour oscillations. Usually however, the infragravity waves will be secondary undulations superimposed on the dominant tidal oscillation. This case can be studied along the lines of this paper too. The frequency spectrum of the tide near the bay entrance is then supposed to contain a continuum part (cf. Munk & Cartwright 1966) besides the peaks at the (low) tidal frequency, including a small-amplitude, but resonating frequency that will be picked out by the bay. The calculations become more involved because one has to include the effect of the tidal water-level change on the eigenmodes of the basin, but in principle the analysis can be performed and is expected to introduce parametric forcing terms (cf. Maas & Doelman 2002, § 5).

The analysis of the nonlinear quarter-wavelength resonances, starts from the shallow-water equations (§ 2). Assuming small amplitudes of the oscillations a perturbation analysis similar to the one employed by Pratt & Llewellyn Smith (1997), is carried out in §3. Starting from the basic state at rest, the first-order equations are linear and yield the quarter-wavelength modes of a half-open basin. Realness of eigenvalues and orthogonality of these first-order eigenmodes can be established, but the amplitude of the resonating mode is still undetermined at this level of description. The linear modes interact at the next (second) order, non-resonantly in our case, leading amongst others to the generation of the zero-frequency mode. The eigenmodes are assumed to be forced (and damped) and interact resonantly only at the next order.† It is thus at third order that closed-form equations governing the slow evolution of the amplitudes of the quarter-wavelength modes are finally obtained, in the form of Landau equations. This is in contrast with the analysis in Pratt & Llewellyn Smith (1997). Whereas the focus of this paper is on the oscillatory modes, their paper deals primarily with the zero-frequency (in rotating systems: geostrophic) mode. Hence their basic first-order modes are the eigenmodes of an entirely closed basin. Moreover, the presence of the zero-frequency eigenmode causes resonant interactions to occur at second order. In the half-open oscillatory case, one is forced to continue up to higher order to find the amplitude equations and assume friction to be still weaker. On the other hand, by the choice of focusing on the oscillatory modes only, we were able to evaluate the qualitative form of the amplitude equation more explicitly.‡ However, although circumstances can be indicated for which there is no zero-frequency eigenmode, it is likely to exist in many basins. A proper description would combine the approach of Pratt & Llewellyn Smith (1997) for the zero-frequency mode and the one presented here for oscillatory modes. At present, the mathematical problems involved with it remain a challenge to be solved. In this paper, the zero-frequency

† Note that resonance is used in its mathematical meaning here: exact correspondence of forcing frequency and eigenfrequency in the frictionless limit, hence giving rise to infinite amplification, i.e. the necessity to remove secular terms.

‡ Compare the final equation (3.28) in this paper with the amplitude equation (3.5) in Pratt & Llewellyn Smith (1997); the latter is the second-order equivalent of (3.21) in this paper.

https://doi.org/10.1017/S0022112004001223 Published online by Cambridge University Press

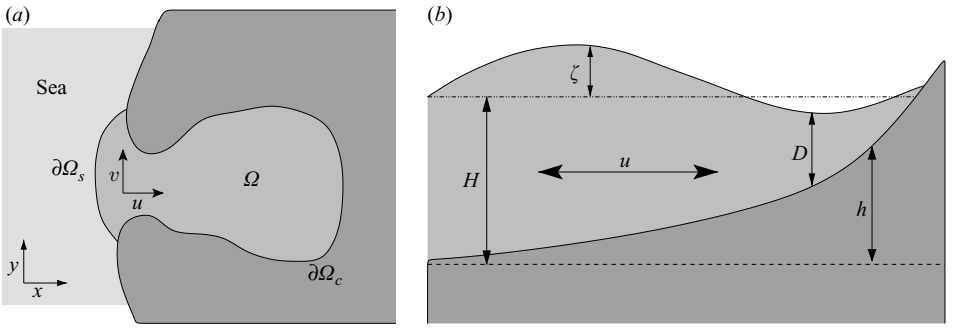


FIGURE 1. Sketch of the tidal basin. (*a*) Top view, (*b*) side view.

eigenmode is simply ignored in order to focus on the interaction between the oscillatory eigenmodes.

Having found the Landau equation describing the (slow) evolution of the amplitudes of the eigen-oscillations of the basin, the behaviour of (solutions of) this equation is analysed further in § 4. The number of modal equations depends on the number of modes that are excited at this order. In § 4 one- and two-mode systems are discussed. The one-mode system is interesting because its amplitude equation is identical to that governing the Helmholtz mode in an almost-enclosed basin, as is found by Maas (1997), Maas & Doelman (2002) and Doelman *et al.* (2002). As the temporal behaviour of the forcing can contain multiple (near-resonant) frequencies, the response of even this single mode can still be quite rich (ranging up to chaotic). However, a complex response can also be facilitated by the interaction between modes, as the two-mode system shows. The paper ends with a discussion of the relevance of the results to the observations in natural basins, and points out certain deficiencies in the theory.

2. Formulation of the model

A tidal basin as shown in figure 1 is considered in this paper. The top view, figure 1(*a*), shows Ω, the area of interest. It is connected to the sea. The seaward boundary of the area Ω is denoted by $\partial\Omega_s$, the coastal boundary by $\partial\Omega_c$. The choice of the precise location of the seaward boundary $\partial\Omega_s$ is somewhat arbitrary and is fixed in time. In the side view, figure 1(*b*), a reference depth H is introduced, chosen to be the undisturbed water depth at sea. The bathymetry is measured relative to this depth level by $h(\boldsymbol{x})$, where $\boldsymbol{x}=(x, y)$ is the horizontal position. The free-surface elevation from the undisturbed water level is denoted by $\zeta(\boldsymbol{x}, t)$. The total instantaneous water depth is thus given by $D(\boldsymbol{x}, t)=H-h(\boldsymbol{x})+\zeta(\boldsymbol{x}, t)$. In fact, the area Ω depends on time. When the water level rises, part of the coast is flooded, increasing the area Ω. The coastal boundary $\partial\Omega_c$ is defined by the condition that the total water depth D is zero, hence is moving in time.†

The water motions are described by the depth-averaged two-dimensional shallow-water equations. They describe the depth-averaged flow of water when the horizontal scales of the motion are much larger than the vertical scale (depth) of the water.

† In principle this gives rise to a slight mismatch between the fixed boundary $\partial\Omega_s$ and the moving boundary $\partial\Omega_c$, so $\partial\Omega_s$ should be lengthened and shortened respectively to keep the connection with $\partial\Omega_c$. These notational futilities do not play a role in this paper however, because the location of $\partial\Omega_c$ is fixed as well to first order of approximation.

https://doi.org/10.1017/S0022112004001223 Published online by Cambridge University Press

Depth-averaged velocities are denoted by $\boldsymbol{U}=(u, v)$. In vectorial form the equations are

$$\frac{\partial \zeta}{\partial t}+\nabla \cdot[D\boldsymbol{U}]=0, \tag{2.1a}$$

$$\frac{\partial \boldsymbol{U}}{\partial t}+[\boldsymbol{U}\cdot\nabla]\boldsymbol{U}+f\hat{\boldsymbol{k}}\times\boldsymbol{U}=-g\nabla\zeta-\frac{\boldsymbol{\tau}_b}{\rho D}, \tag{2.1b}$$

where $\boldsymbol{\tau}_b$ is the bottom friction stress, to be parameterized. Equation (2.1a) is the continuity equation, (2.1b) is the momentum equation. The vector $\hat{\boldsymbol{k}}$ is the vertical unit vector: $\hat{\boldsymbol{k}}\times\boldsymbol{U}=(-v, u)$. These equations are completed with the boundary conditions

$$\frac{\partial D}{\partial t}+[\boldsymbol{U}\cdot\nabla]D=0 \quad \text{at} \quad \partial\Omega_c. \tag{2.2a}$$

$$\zeta=\zeta_e(\boldsymbol{x}, t) \quad \text{at} \quad \partial\Omega_s. \tag{2.2b}$$

At the seaward boundary the free-surface elevation is prescribed to follow the exterior tide $\zeta_e(\boldsymbol{x}, t)$, i.e. radiation damping is not taken into account explicitly. If one intends to properly incorporate this effect, the following considerations could be helpful: (a) Including radiation damping effectively boils down to correcting the exterior tide $\zeta_e(\boldsymbol{x}, t)$ for the waves leaving the basin. Although this correction is important when trying to model the response of a particular basin to a certain exterior forcing, our model still describes the processes in the basin subject to the (possibly corrected) exterior tide $\zeta_e(\boldsymbol{x}, t)$ accurately. In other words, ζ_e describes the water level at sea when the basin is present (i.e. after correcting for radiation damping, although it is not done in this paper), not the tide that would be present if the basin were not there at all. (b) Radiation damping usually leads to linear damping terms in the seaward boundary condition, see e.g. Miles (1971), Garrett (1975), LeBlond & Mysak (1978), Zimmerman (1992) and Nycander & Döös (2001). Because the focus of this work is on nonlinear dynamics, a detailed investigation of radiation damping is beyond the scope of this paper. In the present weakly nonlinear context, it would simply lead to an additional contribution to the linear friction term in the Landau equations.

The condition at the coastal boundary states that $\partial\Omega_c$ is a material boundary, i.e. $\partial\Omega_c$ is a moving boundary whose location varies due to the motion of the fluid. The condition is that particles forming the boundary, which is defined by the condition $D=0$, remain at the boundary. For vertical sidewalls, the local gradient of the depth profile D is infinite. In that case, the appropriate condition is to require the normal component of the velocity to vanish. In this paper condition (2.2a) is used. The alterations for vertical sidewalls are straightforward and do not influence the nature of the results.

A common parametrization for the bottom friction is the quadratic Chezy law $\tau_b=\rho c_D|\boldsymbol{U}|\boldsymbol{U}$, in which $c_D\sim 0.0025$ is a dimensionless drag coefficient (Parker 1991, p. 247). This parameterization could be used here as well. However, in order to simplify the calculations a linear parameterization $\tau_b=\rho r_*\boldsymbol{U}$ will be used. In this so-called Lorentz-linearization the friction parameter r_* should be chosen such that the tidally averaged dissipation of energy is the same for both parameterizations, see Lorentz (1922) and Zimmerman (1992). Note that the results in this paper would be the same if the Chezy law were used. In that case the Taylor series expansion for $|\boldsymbol{U}|\boldsymbol{U}$ must be used, in which the even powers are absent (Dronkers 1962, 1964; Le Provost 1973; Kabbaj & Le Provost 1980). The first term in this expansion corresponds to the linear

https://doi.org/10.1017/S0022112004001223 Published online by Cambridge University Press

friction law used in this paper, whereas the cubic term enters the calculation only at higher order.

3. Derivation of the Landau equations

A weakly nonlinear analysis is carried out, so the amplitude of the motion is assumed to be small. This is incorporated in the equations by scaling the hydrodynamic variables with a small parameter. It is convenient to bring (2.1) and (2.2) into non-dimensional form first. The scalings that are used are

$$\left.\begin{aligned} &\zeta = Z\zeta', \quad D = HD', \quad h = Hh', \\ &x = Lx', \quad y = Ly', \qquad t = \frac{T}{2\pi}t', \quad \boldsymbol{U} = \frac{2\pi L}{T}\frac{Z}{H}\boldsymbol{U}'. \end{aligned}\right\} \tag{3.1}$$

In these expressions, Z is a measure of the amplitude of the free-surface elevation; $\alpha = Z/H$, the non-dimensional amplitude of the tidal motion, is assumed to be small. The non-dimensional depth is $D' = 1 - h' + \alpha\zeta'$. L and T are the length and time scale of the motion. A sensible choice for L would be the length of the basin and for T the period of the main component of the exterior tide, in the tidal case. In the case of secondary undulations, the eigenperiod of the basin would be a more appropriate time scale.

Apart from assuming small amplitude $\alpha \ll 1$, some additional assumptions are necessary in order to obtain a tractable, consistently balanced model. The parameter α will be used as a scaling parameter to reflect these assumptions. For mathematical convenience a single small parameter is used without implying a physical relationship with basin amplitude Z. The scaling assumptions are equivalent to the ones used in Maas & Doelman (2002) and Doelman *et al.* (2002) for Helmholtz basins and correspond to significant degeneration: under these conditions all processes enter the equation at the same order of approximation. First, the system is assumed to be in resonance. Hence the exterior tide will be amplified in the interior. The exterior tide is scaled by α^3, assuming an amplification factor of α^{-2}. This assumption implies that non-resonant components will not play a role at first order. Secondly, the friction parameter $r_* = \alpha^2\sigma H r$ is assumed to be $O(\alpha^2)$, i.e. very small as well. Note that, in view of Lorentz's linearization principle, r_* is expected to depend linearly on the velocity amplitude. The scaling with α^2 instead of α is obtained when assuming the drag coefficient c_D to be $O(\alpha)$. The main motivation is mathematical though: this choice leads to the significant degeneration in which friction enters the equation to balance the nonlinear terms.

After removing the primes, the scaling (3.1) leads to

$$\frac{\partial\zeta}{\partial t} + \nabla\cdot[D\boldsymbol{U}] = 0, \tag{3.2a}$$

$$\frac{\partial\boldsymbol{U}}{\partial t} + \alpha[\boldsymbol{U}\cdot\nabla]\boldsymbol{U} + F\hat{\boldsymbol{k}}\times\boldsymbol{U} = -\gamma\nabla\zeta - \alpha^2 r\frac{\boldsymbol{U}}{D}, \tag{3.2b}$$

where $F = f/\sigma$ is the scaled Coriolis parameter and $\gamma = gH/(\sigma^2L^2)$, acting as the non-dimensional gravitational acceleration, is (the square of) the ratio between the free tidal wavelength and the length scale of the basin. The scaled version of the boundary conditions is

$$\frac{\partial\zeta}{\partial t} + \alpha[\boldsymbol{U}\cdot\nabla]\zeta = [\boldsymbol{U}\cdot\nabla]h \quad \text{at} \quad \partial\Omega_c, \tag{3.3a}$$

$$\zeta = \alpha^2\zeta_e(\boldsymbol{x}, t) \quad \text{at} \quad \partial\Omega_s. \tag{3.3b}$$

https://doi.org/10.1017/S0022112004001223 Published online by Cambridge University Press

Equations (3.2), with (3.3), will be solved by an asymptotic multiple-time-scale expansion in terms of the small amplitude $\alpha \ll 1$: substitute

$$\left.\begin{aligned}\zeta(\boldsymbol{x},t) &= \zeta^{(1)}(\boldsymbol{x},t,\tau)+\alpha\zeta^{(2)}(\boldsymbol{x},t,\tau)+\alpha^2\zeta^{(3)}(\boldsymbol{x},t,\tau)+\ldots,\\ \boldsymbol{U}(\boldsymbol{x},t) &= \boldsymbol{U}^{(1)}(\boldsymbol{x},t,\tau)+\alpha\boldsymbol{U}^{(2)}(\boldsymbol{x},t,\tau)+\alpha^2\boldsymbol{U}^{(3)}(\boldsymbol{x},t,\tau)+\ldots,\end{aligned}\right\} \tag{3.4}$$

in (3.2). The functions $\zeta^{(n)}$ and $\boldsymbol{U}^{(n)}$ depend on the spatial variable $\boldsymbol{x}$, time t and a slow time scale $\tau=\alpha^2 t$. The equations for the evolution of those functions will be derived in subsequent sections by collecting terms of equal order in α in (3.2) and (3.3). It will be found in § 3.2 that the derivatives are zero on the time scale αt, so the time scale τ is the first slow time scale on which evolution is possible, due to the (scaling) assumptions in this paper.

3.1. *First-order solutions*

The first-order equations are

$$\frac{\partial\zeta^{(1)}}{\partial t}+\nabla\cdot\left[D^{(0)}\boldsymbol{U}^{(1)}\right]=0, \tag{3.5a}$$

$$\frac{\partial\boldsymbol{U}^{(1)}}{\partial t}+F\hat{\boldsymbol{k}}\times\boldsymbol{U}^{(1)}=-\gamma\nabla\zeta^{(1)}, \tag{3.5b}$$

where the notation $D^{(0)}(\boldsymbol{x})=1-h(\boldsymbol{x})$ has been introduced. The corresponding boundary conditions are

$$\frac{\partial\zeta^{(1)}}{\partial t}=\left[\boldsymbol{U}^{(1)}\cdot\nabla\right]h \quad \text{at} \quad \partial\Omega_c{}^{(0)}, \tag{3.6a}$$

$$\zeta^{(1)}=0 \quad \text{at} \quad \partial\Omega_s{}^{(0)}. \tag{3.6b}$$

The boundary $\partial\Omega_c{}^{(0)}$ is the fixed boundary at which the still water depth $D^{(0)}$ vanishes, $\partial\Omega_s{}^{(0)}$ is the fixed seaward boundary. Note that $\partial\Omega_s{}^{(0)}$ could be replaced by $\partial\Omega_s$ since the location of this part of the boundary is fixed.

The linear equations (3.5) and (3.6) allow separation of the temporal and spatial behaviour of the solutions. Thus, we write

$$\left.\begin{aligned}\zeta^{(1)}(\boldsymbol{x},t,\tau) &= \sum_j A_j(\tau)\zeta_j(\boldsymbol{x})\mathrm{e}^{\mathrm{i}\omega_j t},\\ \boldsymbol{U}^{(1)}(\boldsymbol{x},t,\tau) &= \sum_j A_j(\tau)\boldsymbol{U}_j(\boldsymbol{x})\mathrm{e}^{\mathrm{i}\omega_j t},\end{aligned}\right\} \tag{3.7}$$

in which summation is over all eigenmodes of the system (3.8) below. The functions $\zeta_j, \boldsymbol{U}_j$ are the eigenfunctions corresponding to the eigenvalues ω_j. The eigenvalues ω_j will be shown to be real-valued, hence correspond to the angular frequency of the jth eigenmode. The amplitudes A_j are constant to first order; the temporal behaviour of (3.7) on the fast time scale t is determined by the eigenfrequencies ω_j. On the slow time scale $\tau=\alpha^2 t$ however, the amplitudes are still allowed to vary. Their evolution depends on higher-order nonlinear interactions between the eigenmodes. In §3.3 the evolution equations, which form the central goal of this paper, for the amplitudes A_j on the slow time scale τ are derived.

The eigenmodes $\zeta_j, \boldsymbol{U}_j, \omega_j$ should satisfy

$$\mathrm{i}\omega_j\zeta_j+\nabla\cdot\left[D^{(0)}\boldsymbol{U}_j\right]=0, \tag{3.8a}$$

$$\mathrm{i}\omega_j\boldsymbol{U}_j+F\hat{\boldsymbol{k}}\times\boldsymbol{U}_j=-\gamma\nabla\zeta_j, \tag{3.8b}$$

https://doi.org/10.1017/S0022112004001223 Published online by Cambridge University Press

together with the boundary equations

$$\mathrm{i}\omega_j\zeta_j = [\boldsymbol{U}_j\cdot\nabla]h \quad \text{at} \quad \partial\Omega_c{}^{(0)}, \tag{3.9a}$$

$$\zeta_j = 0 \quad \text{at} \quad \partial\Omega_s{}^{(0)}. \tag{3.9b}$$

Instead of trying to solve these equations for explicit examples of tidal basins (shape Ω and depth profile $D^{(0)}$, see § 3.4 however), more general results will be derived in this paper, based on the assumption that we have solved (3.8), (3.9). Moreover, a few generic assumptions (3.12) on the set of eigenmodes and eigenvalues are made. Because it is easier to formulate those assumptions having gathered some basic information about the solutions of the eigenvalue problem (3.8), (3.9), their formulation is postponed till the end of this section.

Let $\zeta_j, \boldsymbol{U}_j$ be eigenfunctions of (3.8) with eigenvalue ω_j, and $\zeta_k, \boldsymbol{U}_k$ be eigenfunctions with eigenvalue ω_k. Following Pratt & Llewellyn Smith (1997), consider the following 'generalized inner product'† with the equations

$$\gamma\zeta_k^*\ \mathrm{cont}_j^{(1)} + \gamma\zeta_j\ \mathrm{cont}_k^{(1)*} + D^{(0)}\boldsymbol{U}_k^*\ \cdot\ \mathrm{mom}_j^{(1)} + D^{(0)}\boldsymbol{U}_j\ \cdot\ \mathrm{mom}_k^{(1)*},$$

where $\mathrm{cont}_j^{(1)}$ denotes the continuity equation (3.8*a*) for the jth eigenmode, $\mathrm{cont}_k^{(1)*}$ is its complex conjugate for the kth eigenmode. Analogously, $\mathrm{mom}_j^{(1)}$ and $\mathrm{mom}_k^{(1)*}$ denote the (complex conjugate) momentum equation (3.8*b*), for eigenmodes j and k respectively. This leads to

$$\mathrm{i}(\omega_j-\omega_k^*)\left(\gamma\zeta_k^*\zeta_j + D^{(0)}\boldsymbol{U}_k^*\cdot\boldsymbol{U}_j\right) + \nabla\cdot\left[\gamma D^{(0)}(\zeta_k^*\boldsymbol{U}_j + \zeta_j\boldsymbol{U}_k^*)\right] = 0.$$

Integrating this over the still water area $\Omega^{(0)}$ of the basin, yields the interesting 'inner product equation'

$$(\omega_j-\omega_k^*)\iint_{\Omega^{(0)}}\left(\gamma\,\zeta_k^*\zeta_j + D^{(0)}\,\boldsymbol{U}_k^*\cdot\boldsymbol{U}_j\right)\mathrm{d}x\,\mathrm{d}y = 0. \tag{3.10}$$

The divergence term results in an integral over the boundary $\partial\Omega^{(0)}$ of $\gamma D^{(0)}(\zeta_k^*\boldsymbol{U}_j + \zeta_j\boldsymbol{U}_k^*)\cdot\hat{\boldsymbol{n}}$, with $\hat{\boldsymbol{n}}$ the outward normal along $\partial\Omega^{(0)}$. Using the boundary condition (3.9) for ζ_j and its complex conjugate for ζ_k^* we see that this integral vanishes. Note that $D^{(0)} = 0$ on $\partial\Omega_c{}^{(0)}$.

In analogy with the arguments in Pratt & Llewellyn Smith (1997), some important conclusions can be drawn from (3.10). First, choosing $k = j$ implies that $\omega_j = \omega_j^*$, hence the eigenfrequencies ω_j are real. Because the temporal behaviour of the eigenmodes is $\mathrm{e}^{\mathrm{i}\omega_j t}$, it is purely periodic without decay. Note that the eigenfunctions cannot be chosen to be real-valued, i.e. there will be phase differences within the basin. This is a consequence of the Coriolis acceleration. Moreover, comparing (3.8), (3.9) with their complex conjugate counterparts, it can be concluded that if $\zeta_j, \boldsymbol{U}_j$ are eigenfunctions corresponding to eigenvalue ω_j, then $\zeta_j^*, \boldsymbol{U}_j^*$ are eigenfunctions corresponding to eigenvalue $-\omega_j$. Therefore, it is possible to distinguish the eigenfrequencies $\omega_j \geqslant 0$ and consider the negative ones as complex conjugates of the positive eigenvalues. If the positive eigenvalues are indexed by positive j, it is convenient to let $\omega_{-j} = -\omega_j$ denote the conjugate eigenvalue. Moreover, they can be numbered in increasing order, $\omega_k \geqslant \omega_j$ if $k \geqslant j$.

The second conclusion to be drawn from (3.10) is that the eigenfunctions corresponding to different eigenvalues are orthogonal with respect to the following

† This becomes an inner product only after integrating the integrand over $\Omega^{(0)}$.

https://doi.org/10.1017/S0022112004001223 Published online by Cambridge University Press

inner product:

$$\left\langle \begin{pmatrix} \zeta_k \\ \boldsymbol{U}_k \end{pmatrix}; \begin{pmatrix} \zeta_j \\ \boldsymbol{U}_j \end{pmatrix} \right\rangle = \iint_{\Omega^{(0)}} \left(\gamma\, \zeta_k^* \zeta_j + D^{(0)}\, \boldsymbol{U}_k^* \cdot \boldsymbol{U}_j \right) \mathrm{d}x\, \mathrm{d}y. \tag{3.11}$$

Hence, the set of eigenfunctions can be chosen orthonormal. Physically this inner product is just the dimensionless measure of the energy related to the respective eigenmode; the eigenfunctions are normalized with respect to their energetic content. We assume that they form a complete set. This implies that the expansion (3.7) is indeed the general form in which all solutions $\zeta^{(1)}, \boldsymbol{U}^{(1)}$ to (3.5),(3.6) can be written. Note that, although (3.8),(3.9) is not a classical Sturm–Liouville problem because of the boundary conditions, the conclusions drawn in the preceding paragraph are the same.

The analysis in this paper is carried out for the generic situation. In order to exclude some degenerate cases the following assumptions on the set of eigenmodes and eigenfrequencies are made:

$$\text{the eigenfunctions } (\zeta_j(x), \boldsymbol{U}_j(x)) \text{ form a complete set;} \tag{3.12a}$$

$$\text{there are no degenerate eigenvalues: } \omega_k \neq \omega_l; \tag{3.12b}$$

$$\text{there are no second-order resonances: } \omega_k - \omega_l - \omega_m \neq 0; \tag{3.12c}$$

$$\text{there are no non-trivial third-order resonances: } \omega_k - \omega_l - \omega_m \pm \omega_n \neq 0; \tag{3.12d}$$

where the eigenfrequencies ω_j should be ordered as described before and $k > l \geqslant m \geqslant n \geqslant 1$. Note that (3.12*b*) is implied by (3.12*d*) through considering it for m equal to n. Trivial third-order resonances exist for $k = l$ (contrasting with $k > l$ in the assumption) and $m = n$. Generically the conditions (3.12) are met: situations in which second- or third-order resonances are present are exceptional in the sense that slight changes of the basin, hence the eigenfrequencies, would cause the resonances to disappear. In particular cases for which the assumptions are not satisfied, the forthcoming analysis should be carried out more carefully. In § 3.4 three examples are given and the assumptions are checked.

Remark (zero-frequency mode): The eigenvalue problem (3.8), (3.9) may have a continuum of solutions for $\omega_0 = 0$. For $F \neq 0$ the momentum equation shows that $\gamma\zeta_0/F$ serves as a streamfunction. From the continuity equation it subsequently follows that ζ_0 should be constant along depth contours. Because of the boundary condition at $\partial\Omega_s^{(0)}$, $\zeta_0 = 0$ along depth contours that intersect $\partial\Omega_s^{(0)}$, whereas the boundary condition at $\partial\Omega_c^{(0)}$ implies that $\boldsymbol{U}_0 = 0$ (whence $\nabla\zeta_0 = 0$) along those intersecting $\partial\Omega_c^{(0)}$. So $\omega_j = 0$ is not an eigenvalue unless there are closed depth contours (in the case of a separate crest or trough) in the interior Ω of the basin. On the other hand, if the Coriolis acceleration is negligible, i.e. if $F = 0$ at this order, then $\zeta_0 \equiv 0$ everywhere, whereas $\boldsymbol{U}_0$ is completely free as long as $D^{(0)}\boldsymbol{U}_0$ has zero divergence.

The calculations are much more elaborate if this zero-frequency mode consisting of a continuum of solutions is present. A method to analyse the evolution of this mode by considering circulation integrals is developed by Pratt & Llewellyn Smith (1997) and Pratt (1997). In their work the geostrophic mode (with $\omega_0 = 0$, for $F \neq 0$) is considered, whereas the oscillatory modes play a minor role. The evolution equations, with quadratic nonlinearities, essentially amount to quasi-geostrophic theory for the zero-mode.

https://doi.org/10.1017/S0022112004001223 Published online by Cambridge University Press

Because the focus is on the oscillatory modes and the interactions between them, the zero-mode is omitted in this paper without further justification. Combining the zero-mode and oscillatory modes in a single theory leads to a fundamentally different regime, beyond the scope of this paper. For the terms to balance at the right order, one can argue that the zero-mode should appear only at $O(\alpha^2)$, resonantly forced by quadratic self-interaction of oscillatory modes (note that non-resonant forcing at zero frequency is taken into account in § 3.2). Moreover it could potentially cause much richer (chaotic) behaviour because it interacts quadratically with the oscillatory modes, effectively introducing parametric forcing terms in the Landau equation (3.28) for those modes; this is similar to the effect of the Earth's rotation (see § 4.4.2) in that it invalidates the arguments in § 4.1.

Remark (vertical sidewalls): The only change for the case of vertical sidewalls is the boundary condition at $\partial\Omega_c$. Instead of (3.3*a*), (3.6*a*) and (3.9*a*) one has $\boldsymbol{U}\cdot\hat{\boldsymbol{n}}=0$, $\boldsymbol{U}^{(1)}\cdot\hat{\boldsymbol{n}}=0$ and $\boldsymbol{U}_j\cdot\hat{\boldsymbol{n}}=0$ respectively. Apart from modifying the eigenvalue problem to be solved, this has no influence on the analysis in this paper. The boundary condition at $\partial\Omega_c{}^{(0)}$ was used in the argument following (3.10) showing the integral of $\gamma D^{(0)}(\zeta_k^*\boldsymbol{U}_j+\zeta_j\boldsymbol{U}_k^*)\cdot\hat{\boldsymbol{n}}$ over the boundary $\partial\Omega_c{}^{(0)}$ to be zero because $D^{(0)}=0$. For vertical sidewalls, $D^{(0)}\neq 0$ at $\partial\Omega_c{}^{(0)}$, but $\boldsymbol{U}_j\cdot\hat{\boldsymbol{n}}$ and its complex conjugate are zero, which leads to the same conclusion.

The boundary $\partial\Omega_c$ is not moving, but fixed at vertical sidewalls. The moving boundary causes additional terms in the boundary conditions at higher order. They do not play a role however in the analysis in this paper. At higher order integrals over $\partial\Omega^{(0)}$, similar to the one found in this section, appear. The integrals over $\partial\Omega_c{}^{(0)}$ are zero because $D^{(0)}=0$. For vertical sidewalls, when this is not the case, the boundary condition $\boldsymbol{U}\cdot\hat{\boldsymbol{n}}=0$ implies that the integrals are zero in that case as well.

3.2. *Second-order corrections*

Having solved the first-order equations (3.5), (3.6) by specifying the general solution (3.7), the next step towards the evolution equation for the amplitudes $A_j(\tau)$ is to find the second-order corrections to this approximation. The second-order equations are

$$\frac{\partial\zeta^{(2)}}{\partial t}+\nabla\cdot\left[D^{(0)}\boldsymbol{U}^{(2)}\right]=-\nabla\cdot\left[\zeta^{(1)}\boldsymbol{U}^{(1)}\right], \tag{3.13a}$$

$$\frac{\partial\boldsymbol{U}^{(2)}}{\partial t}+F\hat{\boldsymbol{k}}\times\boldsymbol{U}^{(2)}+\gamma\nabla\zeta^{(2)}=-\left[\boldsymbol{U}^{(1)}\cdot\nabla\right]\boldsymbol{U}^{(1)}. \tag{3.13b}$$

Boundary conditions should be added to these equations. They are different from (3.6) because of the nonlinear terms and due to correction terms for the moving boundary. Because we will expand $\zeta^{(2)}$, $\boldsymbol{U}^{(2)}$ in terms of the first-order eigenmodes and take the inner-product (3.11), it appears that the second-order boundary conditions are not needed. Hence they are omitted. Again it makes sense to take the 'inner product'† with the equations in the form

$$\gamma\zeta_k^*\ \mathrm{cont}^{(2)}+\gamma\zeta^{(2)}\ \mathrm{cont}_k^{(1)*}+D^{(0)}\boldsymbol{U}_k^*\cdot\ \mathrm{mom}^{(2)}+D^{(0)}\boldsymbol{U}^{(2)}\cdot\ \mathrm{mom}_k^{(1)*},$$

where $\mathrm{cont}^{(2)}$ and $\mathrm{mom}^{(2)}$ stand for the continuity and momentum equation (3.13*a*, *b*); $\mathrm{cont}_k^{(1)*}$ and $\mathrm{mom}_k^{(1)*}$, refer to the complex conjugate of (3.8*a*,*b*) as before.This leads

† Again this becomes an inner product only after integrating over $\Omega^{(0)}$.

https://doi.org/10.1017/S0022112004001223 Published online by Cambridge University Press

to the equation

$$\left(\frac{\partial}{\partial t}-\mathrm{i}\omega_k\right)\left(\gamma\zeta_k^*\zeta^{(2)}+D^{(0)}\boldsymbol{U}_k^*\cdot\boldsymbol{U}^{(2)}\right)+\nabla\cdot\left[\gamma D^{(0)}\left(\zeta_k^*\boldsymbol{U}^{(2)}+\zeta^{(2)}\boldsymbol{U}_k^*\right)\right]$$
$$=-\gamma\zeta_k^*\nabla\cdot\left[\zeta^{(1)}\boldsymbol{U}^{(1)}\right]-D^{(0)}\boldsymbol{U}_k^*\cdot\left[\boldsymbol{U}^{(1)}\cdot\nabla\right]\boldsymbol{U}^{(1)}. \quad (3.14)$$

Because the eigenfunctions of (3.8) were assumed to form a complete set, the second-order corrections $\zeta^{(2)}$, $\boldsymbol{U}^{(2)}$ can be expanded in terms of those eigenfunctions, i.e.

$$\left.\begin{aligned}\zeta^{(2)}(\boldsymbol{x},t,\tau)&=\sum_j\tilde{B}_j(t,\tau)\zeta_j(\boldsymbol{x}),\\ \boldsymbol{U}^{(2)}(\boldsymbol{x},t,\tau)&=\sum_j\tilde{B}_j(t,\tau)\boldsymbol{U}_j(\boldsymbol{x}).\end{aligned}\right\} \quad (3.15)$$

The dependence of the amplitudes $\tilde{B}_j$ on the fast time scale t can be found by integrating (3.14) over the still water basin area $\Omega^{(0)}$ to obtain the ordinary differential equation

$$\left(\frac{\partial}{\partial t}-\mathrm{i}\omega_k\right)\tilde{B}_k=-\iint_{\Omega^{(0)}}\left(\gamma\zeta_k^*\nabla\cdot\left[\zeta^{(1)}\boldsymbol{U}^{(1)}\right]+D^{(0)}\boldsymbol{U}_k^*\cdot\left[\boldsymbol{U}^{(1)}\cdot\nabla\right]\boldsymbol{U}^{(1)}\right)\mathrm{d}x\,\mathrm{d}y$$
$$=-\sum_{l,m}({}_k\mathscr{C}_{l,m}+{}_k\mathscr{A}_{l,m})A_lA_m\mathrm{e}^{\mathrm{i}(\omega_l+\omega_m)t}, \quad (3.16)$$

where

$${}_k\mathscr{C}_{l,m}=\iint_{\Omega^{(0)}}\gamma\zeta_k^*\nabla\cdot[\zeta_l\boldsymbol{U}_m]\,\mathrm{d}x\,\mathrm{d}y, \quad (3.17a)$$

$${}_k\mathscr{A}_{l,m}=\iint_{\Omega^{(0)}}D^{(0)}\boldsymbol{U}_k^*\cdot[\boldsymbol{U}_l\cdot\nabla]\boldsymbol{U}_m\,\mathrm{d}x\,\mathrm{d}y \quad (3.17b)$$

are coefficients which can be regarded as inner products of the (normalized) kth eigenvector with the nonlinear terms. Note that the divergence term on the left-hand side of (3.14) integrates to zero again by the same reasoning (following equation (3.10)) as before because $\zeta^{(2)}=0$ on $\partial\Omega_s{}^{(0)}$ as well and $D^{(0)}=0$ on $\partial\Omega_c{}^{(0)}$. This equation can be solved assuming the non-resonance condition (3.12c): $\omega_k\neq\omega_l+\omega_m$, $\forall k,l,m$. Under this assumption the solution of (3.16) is given by

$$\tilde{B}_k(t,\tau)=B_k(\tau)\mathrm{e}^{\mathrm{i}\omega_kt}-\mathrm{i}\sum_{l,m}\frac{{}_k\mathscr{C}_{l,m}+{}_k\mathscr{A}_{l,m}}{\omega_k-\omega_l-\omega_m}A_l(\tau)A_m(\tau)\mathrm{e}^{\mathrm{i}(\omega_l+\omega_m)t}, \quad (3.18)$$

with $B_k(\tau)$ some unknown second-order amplitudes. This expression should be substituted into (3.15) to find the second-order corrections. The non-resonance condition implies that the second-order corrections remain slaved and second order and do not lead to secularities. If the non-resonance condition is not satisfied, then the amplitudes $\tilde{B}_k(t,\tau)$ would increase linearly in time t, violating the regularity of the asymptotic expansion (3.4). In that case a solvability condition should be applied at this order (as is next done in § 3.3) leading to free dynamics of the first-order amplitudes by quadratic interactions (instead of cubic). In general however, the non-resonance condition will be met.

https://doi.org/10.1017/S0022112004001223 Published online by Cambridge University Press

3.3. *Third-order: evolution*

Finally, the equations at third order in α are given by

$$\frac{\partial \zeta^{(1)}}{\partial \tau}+\frac{\partial \zeta^{(3)}}{\partial t}+\nabla\cdot\left[D^{(0)}\boldsymbol{U}^{(3)}\right]=-\nabla\cdot\left[\zeta^{(1)}\boldsymbol{U}^{(2)}+\zeta^{(2)}\boldsymbol{U}^{(1)}\right], \tag{3.19a}$$

$$\frac{\partial \boldsymbol{U}^{(1)}}{\partial \tau}+\frac{\partial \boldsymbol{U}^{(3)}}{\partial t}+F\hat{\boldsymbol{k}}\times\boldsymbol{U}^{(3)}+\gamma\nabla\zeta^{(3)}=-\left[\boldsymbol{U}^{(1)}\cdot\nabla\right]\boldsymbol{U}^{(2)}-\left[\boldsymbol{U}^{(2)}\cdot\nabla\right]\boldsymbol{U}^{(1)}-r\frac{\boldsymbol{U}^{(1)}}{D^{(0)}}. \tag{3.19b}$$

As before, boundary conditions should be added, but they are not needed and hence omitted because we will not try to solve for $\zeta^{(3)}, \boldsymbol{U}^{(3)}$. In addition to the contributions of the nonlinear terms on the right-hand side of these equations, the slow evolution of the first-order solutions appears. In order to find bounded solutions for $\zeta^{(3)}, \boldsymbol{U}^{(3)}$, a solvability condition must be satisfied. This condition yields the slow evolution of the amplitudes $A_k(\tau)$ of the first-order solution, which is determined by friction and the nonlinear interactions. To derive the equation for the slow evolution, consider the 'inner product'

$$\gamma\zeta_k^*\ \mathrm{cont}^{(3)}+\gamma\zeta^{(3)}\ \mathrm{cont}_k^{(1)*}+D^{(0)}\boldsymbol{U}_k^*\cdot\mathrm{mom}^{(3)}+D^{(0)}\boldsymbol{U}^{(3)}\cdot\mathrm{mom}_k^{(1)*},$$

which yields

$$\begin{aligned}&\frac{\partial}{\partial\tau}\left(\gamma\zeta_k^*\zeta^{(1)}+D^{(0)}\boldsymbol{U}_k^*\cdot\boldsymbol{U}^{(1)}\right)+\left(\frac{\partial}{\partial t}-\mathrm{i}\omega_k\right)\left(\gamma\zeta_k^*\zeta^{(3)}+D^{(0)}\boldsymbol{U}_k^*\cdot\boldsymbol{U}^{(3)}\right)\\&\quad+\nabla\cdot\left[\gamma D^{(0)}\left(\zeta_k^*\boldsymbol{U}^{(3)}+\zeta^{(3)}\boldsymbol{U}_k^*\right)\right]\\&=-\gamma\zeta_k^*\nabla\cdot\left[\zeta^{(1)}\boldsymbol{U}^{(2)}+\zeta^{(2)}\boldsymbol{U}^{(1)}\right]-D^{(0)}\boldsymbol{U}_k^*\cdot\left(\left[\boldsymbol{U}^{(1)}\cdot\nabla\right]\boldsymbol{U}^{(2)}+\left[\boldsymbol{U}^{(2)}\cdot\nabla\right]\boldsymbol{U}^{(1)}\right)\\&\quad-r\boldsymbol{U}_k^*\cdot\boldsymbol{U}^{(1)}.\end{aligned} \tag{3.20}$$

When integrating this expression over the still water basin area $\Omega^{(0)}$ to obtain the global energy balance the divergence term on the left-hand side requires special attention: it integrates to

$$\oint_{\partial\Omega^{(0)}}\gamma D^{(0)}\left(\zeta_k^*\boldsymbol{U}^{(3)}+\zeta^{(3)}\boldsymbol{U}_k^*\right)\cdot\hat{\boldsymbol{n}}\,\mathrm{d}s,$$

which can be divided into an integral over $\partial\Omega_c{}^{(0)}$ and an integral over $\partial\Omega_s{}^{(0)}$. The integrand is zero on $\partial\Omega_c{}^{(0)}$ as before, see the discussion following (3.10), but along $\partial\Omega_s{}^{(0)}$ more care has to be taken. In fact, the boundary condition (3.3*b*) leads to $\zeta^{(3)}=\zeta_e$ at $\partial\Omega_s{}^{(0)}$ at third order. Using the fact that $\zeta_k^*=0$ at $\partial\Omega_s{}^{(0)}$, we see that the first part of the integrand still vanishes on $\partial\Omega_s{}^{(0)}$. Therefore, integration of (3.20) over $\Omega^{(0)}$ leads to

$$\begin{aligned}&\left(\frac{\partial}{\partial t}-\mathrm{i}\omega_k\right)\left\langle\begin{pmatrix}\zeta_k\\\boldsymbol{U}_k\end{pmatrix};\begin{pmatrix}\zeta^{(3)}\\\boldsymbol{U}^{(3)}\end{pmatrix}\right\rangle+\frac{\partial}{\partial\tau}\left\langle\begin{pmatrix}\zeta_k\\\boldsymbol{U}_k\end{pmatrix};\begin{pmatrix}\zeta^{(1)}\\\boldsymbol{U}^{(1)}\end{pmatrix}\right\rangle+\int_{\partial\Omega_s{}^{(0)}}\gamma D^{(0)}\zeta_e\boldsymbol{U}_k^*\cdot\hat{\boldsymbol{n}}\,\mathrm{d}s\\&=-\iint_{\Omega^{(0)}}\gamma\zeta_k^*\nabla\cdot\left[\zeta^{(1)}\boldsymbol{U}^{(2)}+\zeta^{(2)}\boldsymbol{U}^{(1)}\right]\mathrm{d}x\,\mathrm{d}y\\&\quad-\iint_{\Omega^{(0)}}D^{(0)}\boldsymbol{U}_k^*\cdot\left(\left[\boldsymbol{U}^{(1)}\cdot\nabla\right]\boldsymbol{U}^{(2)}+\left[\boldsymbol{U}^{(2)}\cdot\nabla\right]\boldsymbol{U}^{(1)}\right)\mathrm{d}x\,\mathrm{d}y-\iint_{\Omega^{(0)}}r\boldsymbol{U}_k^*\cdot\boldsymbol{U}^{(1)}\,\mathrm{d}x\,\mathrm{d}y.\end{aligned}$$

A solvability condition must be satisfied in order for this equation to yield bounded third-order corrections: all terms for which the temporal behaviour on the fast time scale t is given by $\mathrm{e}^{\mathrm{i}\omega_k t}$ must cancel, otherwise $\left\langle\binom{\zeta_k}{\boldsymbol{U}_k};\binom{\zeta^{(3)}}{\boldsymbol{U}^{(3)}}\right\rangle$ will grow due to resonance.

https://doi.org/10.1017/S0022112004001223 Published online by Cambridge University Press

For an efficient evaluation of this condition, the expansions (3.7), (3.15) and (3.18) are substituted. Because of the orthonormality of the eigenfunctions the derivative with respect to τ evaluates to $(\mathrm{d}A_k/\mathrm{d}\tau)\mathrm{e}^{\mathrm{i}\omega_k t}$, whose t-temporal behaviour is clearly resonant. Consequently, the solvability condition reads

$$\begin{aligned}\frac{\mathrm{d}A_k}{\mathrm{d}\tau} = &- \int_{\partial\Omega_s{}^{(0)}} \gamma D^{(0)}\{\zeta_e\}_k \boldsymbol{U}_k^* \cdot \hat{\boldsymbol{n}}\,\mathrm{d}s - \left\{\iint_{\Omega^{(0)}} \gamma\zeta_k^*\nabla\cdot\left[\zeta^{(1)}\boldsymbol{U}^{(2)}+\zeta^{(2)}\boldsymbol{U}^{(1)}\right]\mathrm{d}x\,\mathrm{d}y\right\}_k \\ &- \left\{\iint_{\Omega^{(0)}} D^{(0)}\boldsymbol{U}_k^*\cdot\left(\left[\boldsymbol{U}^{(1)}\cdot\nabla\right]\boldsymbol{U}^{(2)}+\left[\boldsymbol{U}^{(2)}\cdot\nabla\right]\boldsymbol{U}^{(1)}\right)\mathrm{d}x\,\mathrm{d}y\right\}_k \\ &- \left\{\iint_{\Omega^{(0)}} r\boldsymbol{U}_k^*\cdot\boldsymbol{U}^{(1)}\,\mathrm{d}x\,\mathrm{d}y\right\}_k, \end{aligned} \tag{3.21}$$

where $\{\cdot\}_k$ denotes the operator that selects the Fourier component with frequency ω_k, i.e. $\{\mathrm{e}^{\mathrm{i}\omega t}\}_k \sim \delta(\omega-\omega_k)$. Next, each term on the right-hand side of (3.21) will be studied.

For the forcing term, we define

$$F_k(\tau) = -\int_{\partial\Omega_s{}^{(0)}} \gamma D^{(0)}\{\zeta_e(\boldsymbol{x},t,\tau)\}_k \boldsymbol{U}_k^*\cdot\hat{\boldsymbol{n}}\,\mathrm{d}s. \tag{3.22}$$

For single-frequency forcing at one of the resonant frequencies ω_k, i.e. $\zeta_e = \alpha_e\,\mathrm{e}^{\mathrm{i}\omega_k t}$, $\{\zeta_e\}_k = \alpha_e$ is constant, hence $F_k(\tau)\equiv F_k$ is constant as well. For nearly resonant forcing, $F_k(\tau)$ will be periodic, see §4 for more details.

Defining

$$\mathscr{R}_{k,j} = \iint_{\Omega^{(0)}} \boldsymbol{U}_k^*\cdot\boldsymbol{U}_j\,\mathrm{d}x\,\mathrm{d}y \tag{3.23}$$

the frictional term in (3.21) can be rewritten as

$$\sum_j r\mathscr{R}_{k,j}A_j\{\mathrm{e}^{\mathrm{i}\omega_j t}\}_k. \tag{3.24}$$

The summation is over all eigenvalues of (3.8) like in the expansion (3.7). Because friction was linearized in this model, this expression is linear in the amplitudes A_j. Note that $\{\mathrm{e}^{\mathrm{i}\omega_j t}\}_k = \delta_{jk}$, with δ_{jk} the Kronecker delta, because of the assumed non-degeneracy: $\omega_j \neq \omega_k$ if $j\neq k$. This simplification will be used shortly. For a quadratic or cubic friction law, the calculations would be more elaborate, but in principle no more difficult than those for the quadratic nonlinear terms considered in this paper.

Substituting the expansions (3.7), (3.15) and (3.18) into the nonlinear terms of (3.21) leads to

$$\begin{aligned}&-\left\{\iint_{\Omega^{(0)}} \gamma\zeta_k^*\nabla\cdot\left[\zeta^{(1)}\boldsymbol{U}^{(2)}+\zeta^{(2)}\boldsymbol{U}^{(1)}\right]\mathrm{d}x\,\mathrm{d}y\right\}_k \\ &\quad= \left\{\mathrm{i}\sum_j\sum_{n,l,m} A_j\mathrm{e}^{\mathrm{i}\omega_j t}\frac{{}_n\mathscr{C}_{l,m}+{}_n\mathscr{A}_{l,m}}{\omega_n-\omega_l-\omega_m}A_lA_m\mathrm{e}^{\mathrm{i}(\omega_l+\omega_m)t}\iint_{\Omega^{(0)}}\gamma\zeta_k^*\nabla\cdot[\zeta_j\boldsymbol{U}_n+\zeta_n\boldsymbol{U}_j]\,\mathrm{d}x\,\mathrm{d}y\right\}_k \\ &\quad= \mathrm{i}\sum_{j,n,l,m}\frac{{}_n\mathscr{C}_{l,m}+{}_n\mathscr{A}_{l,m}}{\omega_n-\omega_l-\omega_m}({}_k\mathscr{C}_{j,n}+{}_k\mathscr{C}_{n,j})A_jA_lA_m\{\mathrm{e}^{\mathrm{i}(\omega_j+\omega_l+\omega_m)t}\}_k \end{aligned} \tag{3.25}$$

https://doi.org/10.1017/S0022112004001223 Published online by Cambridge University Press

for the continuity term and for the advection

$$-\left\{\iint_{\Omega^{(0)}} D^{(0)}\boldsymbol{U}_k^*\cdot\left(\left[\boldsymbol{U}^{(1)}\cdot\nabla\right]\boldsymbol{U}^{(2)}+\left[\boldsymbol{U}^{(2)}\cdot\nabla\right]\boldsymbol{U}^{(1)}\right)\,\mathrm{d}x\,\mathrm{d}y\right\}_k$$
$$=\mathrm{i}\sum_{j,n,l,m}\frac{{}_n\mathscr{C}_{l,m}+{}_n\mathscr{A}_{l,m}}{\omega_n-\omega_l-\omega_m}({}_k\mathscr{A}_{j,n}+{}_k\mathscr{A}_{n,j})A_jA_lA_m\left\{\mathrm{e}^{\mathrm{i}(\omega_j+\omega_l+\omega_m)t}\right\}_k,\quad(3.26)$$

in which each of the indices j, n, l and m runs over all eigenvalues. Note that the contributions with $B_n(\tau)\mathrm{e}^{\mathrm{i}\omega_n t}$ are omitted because they lead to the selection criterion $\{\mathrm{e}^{\mathrm{i}(\omega_j+\omega_n)t}\}_k$ which is zero due to the assumption (3.12*c*). Combining (3.22), (3.24), (3.25), (3.26) with (3.21) we find the so-called Landau (or amplitude) equation for the slow evolution of the first-order amplitudes:

$$\frac{\mathrm{d}A_k}{\mathrm{d}\tau}=F_k(\tau)-\sum_j r\mathscr{R}_{k,j}\{\mathrm{e}^{\mathrm{i}\omega_j t}\}_kA_j$$
$$+\mathrm{i}\sum_{j,n,l,m}\frac{{}_n\mathscr{N}_{l,m}}{\omega_n-\omega_l-\omega_m}({}_k\mathscr{N}_{j,n}+{}_k\mathscr{N}_{n,j})\left\{\mathrm{e}^{\mathrm{i}(\omega_j+\omega_l+\omega_m)t}\right\}_kA_jA_lA_m,\quad(3.27)$$

where the shorthand notation ${}_k\mathscr{N}_{l,m}={}_k\mathscr{C}_{l,m}+{}_k\mathscr{A}_{l,m}$ was used. Note that the operator $\{\cdot\}_k$ selects the terms in the summation for which $\omega_j=\omega_k$ or $\omega_j+\omega_l+\omega_m=\omega_k$ respectively. Our final step is to evaluate these conditions using the assumptions in (3.12).

First, it has been noted already that the non-degeneracy of the eigenfrequencies implies that $\{\mathrm{e}^{\mathrm{i}\omega_j t}\}_k=\delta_{jk}$, so the friction term reduces to

$$\sum_j r\mathscr{R}_{k,j}A_j\{\mathrm{e}^{\mathrm{i}\omega_j t}\}_k=c_kA_k,$$

defining $c_k=r\mathscr{R}_{k,k}$, which is clearly positive for all k, in view of (3.23).

Secondly, (3.12*d*) helps evaluate the condition $\omega_j+\omega_l+\omega_m=\omega_k$. There are 'trivial' solutions $\omega_j+\omega_{-j}+\omega_k=\omega_k$ to this condition in view of the chosen order of numbering $\omega_{-j}=-\omega_j$, see the discussion following (3.10). These 'trivial resonances' stem from symmetry in the eigenvalue problem (3.8). The assumption (3.12*d*) amounts to assuming that these 'trivial resonances' are the only ones, apart from permutations. In fact, by reformulating the condition in terms of positive eigenfrequencies only, and reordering in such a way that $\omega_k\geqslant\omega_j\geqslant\omega_l\geqslant\omega_m$, the condition reads $\omega_k\pm\omega_j\pm\omega_l\pm\omega_m=0$ without loss of generality. The cases $+++$, $++-$, $+-+$ and $-++$ are ruled out immediately, because the left-hand side is always strictly positive (note that we ordered them such that ω_k is the largest one and $\omega_0=0$ is not considered in this paper). Similarly, the cases $+--$ and $-+-$ can only satisfy the condition in the trivial cases. In the latter case, for example, note that both $\omega_k-\omega_j\geqslant0$ and $\omega_l-\omega_m\geqslant0$, with equality only if $k=j$ and $l=m$, i.e. in the trivial cases. This leaves the cases $--+$ and $---$, for which solutions with $k>j$ are ruled out by (3.12*d*). For $k=j$ it is clear that $\omega_k-\omega_j-\omega_l-\omega_m<0$ does not constitute a solution either. Hence one is left with the trivial cases $\omega_k-\omega_k-\omega_l+\omega_l=0$.

In (3.27) all permutations of j, n, l and m occur as well, so twelve situations can be distinguished in which $\{\mathrm{e}^{\mathrm{i}(\omega_j+\omega_l+\omega_m)t}\}_k\neq0$. The corresponding non-zero terms in the summation over j, n, l and m are shown in table 1. In this table, the indices j, n, l and m are positive; $\bar{m}$ is a shorthand notation for $-m$. Note that $\omega_{\bar{n}}=-\omega_n$ and $A_{\bar{n}}=A_n^*$. The latter follows from equating (3.7) with its complex conjugate, using the fact that $\zeta^{(1)}, \boldsymbol{U}^{(1)}$ are real. Note that all terms are proportional to $|A_m|^2A_k$.

https://doi.org/10.1017/S0022112004001223 Published online by Cambridge University Press

n	j	l	m	Corresponding term
$+$	$+k$	$+m$	$-m$	$\mathrm{i}\frac{1}{\omega_n}\,{}_n\mathcal{N}_{m,\bar{m}}\,({}_k\mathcal{N}_{k,n}+{}_k\mathcal{N}_{n,k})\;A_kA_mA_m^*$
$-$	$+k$	$+m$	$-m$	$-\mathrm{i}\frac{1}{\omega_n}\,{}_{\bar{n}}\mathcal{N}_{m,\bar{m}}\,({}_k\mathcal{N}_{k,\bar{n}}+{}_k\mathcal{N}_{\bar{n},k})\;A_kA_mA_m^*$
$+$	$+k$	$-m$	$+m$	$\mathrm{i}\frac{1}{\omega_n}\,{}_n\mathcal{N}_{\bar{m},m}\,({}_k\mathcal{N}_{k,n}+{}_k\mathcal{N}_{n,k})\;A_kA_m^*A_m$
$-$	$+k$	$-m$	$+m$	$-\mathrm{i}\frac{1}{\omega_n}\,{}_{\bar{n}}\mathcal{N}_{\bar{m},m}\,({}_k\mathcal{N}_{k,\bar{n}}+{}_k\mathcal{N}_{\bar{n},k})\;A_kA_m^*A_m$
$+$	$+m$	$+k$	$-m$	$\mathrm{i}\frac{1}{\omega_n+\omega_m-\omega_k}\,{}_n\mathcal{N}_{k,\bar{m}}\,({}_k\mathcal{N}_{m,n}+{}_k\mathcal{N}_{n,m})\;A_mA_kA_m^*$
$-$	$+m$	$+k$	$-m$	$-\mathrm{i}\frac{1}{\omega_n-\omega_m+\omega_k}\,{}_{\bar{n}}\mathcal{N}_{k,\bar{m}}\,({}_k\mathcal{N}_{m,\bar{n}}+{}_k\mathcal{N}_{\bar{n},m})\;A_mA_kA_m^*$
$+$	$-m$	$+k$	$+m$	$\mathrm{i}\frac{1}{\omega_n-\omega_m-\omega_k}\,{}_n\mathcal{N}_{k,m}\,({}_k\mathcal{N}_{\bar{m},n}+{}_k\mathcal{N}_{n,\bar{m}})\;A_m^*A_kA_m$
$-$	$-m$	$+k$	$+m$	$-\mathrm{i}\frac{1}{\omega_n+\omega_m+\omega_k}\,{}_{\bar{n}}\mathcal{N}_{k,m}\,({}_k\mathcal{N}_{\bar{m},\bar{n}}+{}_k\mathcal{N}_{\bar{n},\bar{m}})\;A_m^*A_kA_m$
$+$	$+m$	$-m$	$+k$	$\mathrm{i}\frac{1}{\omega_n+\omega_m-\omega_k}\,{}_n\mathcal{N}_{\bar{m},k}\,({}_k\mathcal{N}_{m,n}+{}_k\mathcal{N}_{n,m})\;A_mA_m^*A_k$
$-$	$+m$	$-m$	$+k$	$-\mathrm{i}\frac{1}{\omega_n-\omega_m+\omega_k}\,{}_{\bar{n}}\mathcal{N}_{\bar{m},k}\,({}_k\mathcal{N}_{m,\bar{n}}+{}_k\mathcal{N}_{\bar{n},m})\;A_mA_m^*A_k$
$+$	$-m$	$+m$	$+k$	$\mathrm{i}\frac{1}{\omega_n-\omega_m-\omega_k}\,{}_n\mathcal{N}_{m,k}\,({}_k\mathcal{N}_{\bar{m},n}+{}_k\mathcal{N}_{n,\bar{m}})\;A_m^*A_mA_k$
$-$	$-m$	$+m$	$+k$	$-\mathrm{i}\frac{1}{\omega_n+\omega_m+\omega_k}\,{}_{\bar{n}}\mathcal{N}_{m,k}\,({}_k\mathcal{N}_{\bar{m},\bar{n}}+{}_k\mathcal{N}_{\bar{n},\bar{m}})\;A_m^*A_mA_k$

TABLE 1. Systematic list of non-zero nonlinear terms assuming 'trivial resonances' only.

Summing the terms in table 1 finally leads to the following simplified Landau equation:

$$\frac{\mathrm{d}A_k}{\mathrm{d}\tau}=F_k(\tau)-c_k\,A_k+\sum_m \mathrm{i}\,\Gamma_{k,m}\;A_m^*A_mA_k \tag{3.28}$$

with coefficient $\Gamma_{k,m}$ in the nonlinear term given by

$$\begin{aligned}\Gamma_{k,m}=&\sum_{n\geqslant 1}\frac{1}{\omega_n}({}_k\mathcal{N}_{k,n}+{}_k\mathcal{N}_{n,k})({}_n\mathcal{N}_{m,\bar{m}}+{}_n\mathcal{N}_{\bar{m},m})-\frac{1}{\omega_n}({}_k\mathcal{N}_{k,\bar{n}}+{}_k\mathcal{N}_{\bar{n},k})({}_{\bar{n}}\mathcal{N}_{m,\bar{m}}+{}_{\bar{n}}\mathcal{N}_{\bar{m},m})\\&+\frac{1}{\omega_n+\omega_m-\omega_k}({}_k\mathcal{N}_{m,n}+{}_k\mathcal{N}_{n,m})({}_n\mathcal{N}_{k,\bar{m}}+{}_n\mathcal{N}_{\bar{m},k})\\&-\frac{1}{\omega_n-\omega_m+\omega_k}({}_k\mathcal{N}_{m,\bar{n}}+{}_k\mathcal{N}_{\bar{n},m})({}_{\bar{n}}\mathcal{N}_{k,\bar{m}}+{}_{\bar{n}}\mathcal{N}_{\bar{m},k})\\&+\frac{1}{\omega_n-\omega_m-\omega_k}({}_k\mathcal{N}_{\bar{m},n}+{}_k\mathcal{N}_{n,\bar{m}})({}_n\mathcal{N}_{k,m}+{}_n\mathcal{N}_{m,k})\\&-\frac{1}{\omega_n+\omega_m+\omega_k}({}_k\mathcal{N}_{\bar{m},\bar{n}}+{}_k\mathcal{N}_{\bar{n},\bar{m}})({}_{\bar{n}}\mathcal{N}_{k,m}+{}_{\bar{n}}\mathcal{N}_{m,k}).\end{aligned} \tag{3.29}$$

https://doi.org/10.1017/S0022112004001223 Published online by Cambridge University Press

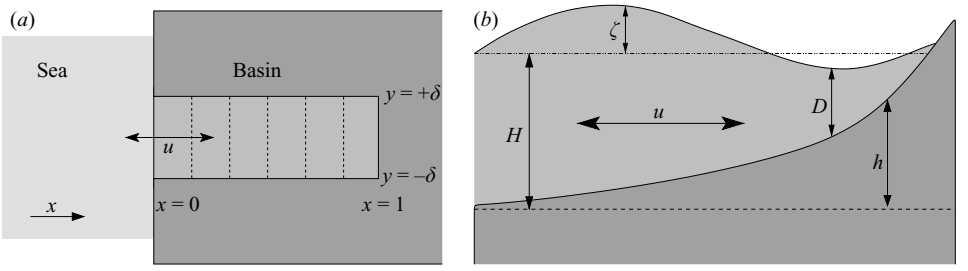


FIGURE 2. Sketch of the one-dimensional basin. Its width is much smaller than its length, the bottom profile $h(x)$ depends on the longitudinal coordinate only, and hence the motion is assumed to be restricted to the longitudinal direction. (*a*) Top view, (*b*) side view.

In (3.28) we have essentially separated the slow evolution of the amplitudes from the dependence of the hydrodynamic system on the geometry of the basin (from its 'fast' oscillatory eigenmodes in particular). All information about the geometry of the basin is contained in the coefficients c_k and $\Gamma_{k,m}$. The geometry of the basin determines the eigenvalues and eigenfunctions, hence the coupling coefficients $\mathscr{R}_{k,j}$, ${}_k\mathscr{C}_{l,m}$, ${}_k\mathscr{A}_{l,m}$ and $\{e^{i(\omega_j+\omega_l+\omega_m)t}\}_k$, which finally give c_k and $\Gamma_{k,m}$. Once these coefficients are fixed, the dynamical system given by (3.28) can be studied. From the definition (3.23) for the coefficient $\mathscr{R}_{k,k}$ it is clear that $c_k > 0$. Omitting the Coriolis acceleration ($F = 0$), the coefficients $\Gamma_{k,m}$ can be shown to be real-valued. The reason for this is that the eigenfunctions ζ_j can be chosen real-valued in that case, whereas the corresponding velocities $\boldsymbol{U}_j$ will be imaginary. Therefore ${}_k\mathscr{N}_{l,m} = {}_k\mathscr{C}_{l,m} + {}_k\mathscr{A}_{l,m}$ is imaginary for all indices k, l, m, in view of the definitions (3.17).

3.4. *Some example bedforms*

In order to illustrate the derivation and obtain some knowledge about the order of magnitude of the coefficients $\Gamma_{k,m}$ three relatively simple examples are worked out. For simplicity, rectangular basins are considered for which the width is much smaller than the length of the basin, see figure 2. As a consequence the motion can be assumed to be one-dimensional, uniform in the transverse direction; the transverse velocities are zero. Indeed, rescaling $y \mapsto \delta y$, $v \mapsto \delta v$ and introducing an asymptotic expansion in terms of the Kelvin number δF, where $\delta \ll 1$ is the width over length aspect ratio, it readily follows that up to first order $v = 0$ and the equations (3.8),(3.9), describing the linear free modes of the system, reduce to (see e.g. Krauss 1973, pp. 154–155)

$$\gamma \frac{\mathrm{d}}{\mathrm{d}x}\left[(1-h(x))\,\frac{\mathrm{d}\zeta_j}{\mathrm{d}x}\right] + {\omega_j}^2\,\zeta_j = 0 \quad \text{for} \quad x \in [0,1], \tag{3.30a}$$

$$\zeta_j = 0 \quad \text{at} \quad x = 0, \tag{3.30b}$$

$$\gamma\,(1-h(x))\,\frac{\mathrm{d}^2\zeta_j}{\mathrm{d}x^2} = 0 \quad \text{at} \quad x = 1, \tag{3.30c}$$

after eliminating the longitudinal velocity component $u_j = \mathrm{i}(\gamma/\omega_j)(\mathrm{d}\zeta_j/\mathrm{d}x)$. Note that the coastal boundary condition (3.30*c*) should be interpreted to require $\mathrm{d}^2\zeta_j/\mathrm{d}x^2$ to be bounded for vanishing depth (if $h(1) = 1$). Three examples will be discussed here: the basin with constant depth, $h(x) \equiv 0$; a basin with constant slope, $h(x) = x$; and a basin with a quadratically sloping bottom, $h(x) = x^2$. This results in standard

https://doi.org/10.1017/S0022112004001223 Published online by Cambridge University Press

equations whose solutions are given by either

$$\left.\begin{aligned} \zeta_j(x) &= (1/\sqrt{\gamma})\,\sin\left(\left(j+\tfrac{1}{2}\right)\pi x\right),\\ u_j(x) &= \mathrm{i}\,\cos\left(\left(j+\tfrac{1}{2}\right)\pi x\right),\\ \omega_j &= \left(j+\tfrac{1}{2}\right)\pi\sqrt{\gamma}, \end{aligned}\right\} \tag{3.31}$$

for constant depth (with boundary condition $\mathrm{d}\zeta_j/\mathrm{d}x = 0$, at $x = 1$, because in this case the wall is vertical),

$$\left.\begin{aligned} \zeta_j(x) &= \frac{J_0(p_j\sqrt{1-x})}{\sqrt{2\gamma}\,J_1(p_j)},\\ u_j(x) &= \mathrm{i}\frac{J_1(p_j\sqrt{1-x})}{\sqrt{2}\,J_1(p_j)\sqrt{1-x}},\\ \omega_j &= \frac{1}{2}\sqrt{\gamma}\,p_j, \end{aligned}\right\} \tag{3.32}$$

for constant slope, where J_0 and J_1 are Bessel functions of the first kind and p_j the positive roots of J_0, or

$$\left.\begin{aligned} \zeta_j(x) &= \sqrt{\frac{4j-1}{2\gamma}}\,P_{2j-1}(x),\\ u_j(x) &= \mathrm{i}\sqrt{\frac{(4j-1)(2j-1)}{4j}}\,\frac{P_{2j-2}(x)-xP_{2j-1}(x)}{1-x^2},\\ \omega_j &= \sqrt{\gamma}\sqrt{2j(2j-1)}, \end{aligned}\right\} \tag{3.33}$$

for the quadratically sloping bottom, where P_{2j-1} is the Legendre polynomial of degree $2j-1$. These eigenfunctions are normalized with respect to the inner product (3.11).

For these examples, the assumptions (3.12) can be checked. The eigenvalues are non-degenerate in all cases. The completeness of the eigenfunctions follows from standard expansion theorems for Fourier series, Bessel functions and Legendre polynomials. The remaining two assumptions need some more attention. For the basin with constant depth we find that $\omega_k - \omega_l - \omega_m = (k-l-m-\frac{1}{2})\pi\sqrt{\gamma}$, which clearly is non-zero, because $k-l-m$ is an integer. The final condition however, $0 = \omega_k - \omega_l - \omega_m \pm \omega_n = (k-l-m\pm n-\frac{1}{2}\pm\frac{1}{2})\pi\sqrt{\gamma}$ is fulfilled whenever $k = l+m-n$ or $k = l+m+n+1$ respectively; many non-trivial resonances occur for this basin. Apparently the special symmetries of this basin cause the resonance condition to be fulfilled even though they are not generic.

In order to check the non-resonance conditions (3.12*c*,*d*) for $\omega_j = \frac{1}{2}\sqrt{\gamma}\,p_j$ and $\omega_j = \sqrt{\gamma}\sqrt{2j(2j-1)}$, for the linear and quadratic bottom respectively, an approximation of the eigenfrequencies is helpful. In fact, the approximations for both cases are very similar:

$$\varpi_j = a\left(j-\frac{1}{4}\right) - \frac{1}{4j-1} + \frac{\chi_j}{(4j-1)^3} \tag{3.34}$$

where $\varpi_j = -4\pi\omega_j/\sqrt{\gamma}$, $a = -2\pi^2$ and $0.3089 < \chi_j < 31/(3\pi^2)$, in the case of a linearly sloping bottom, or $\varpi_j = 4\omega_j/\sqrt{\gamma}$, $a = 8$ and $\frac{1}{4} < \chi_j < \frac{27}{128}\sqrt{2}$, in the case of a quadratic bottom. For the linear bottom this approximation is McMahon's expansion for zeros

https://doi.org/10.1017/S0022112004001223 Published online by Cambridge University Press

of Bessel functions (see Gatteschi & Giordano 2000, (6) or Theorem 4), for the second case it follows from a Taylor expansion of $\sqrt{2j(2j-1)} = (2j-\frac{1}{2})\sqrt{1-(4j-1)^{-2}}$. The estimate (3.34) is sufficient to prove both non-resonance conditions (3.12*c*,*d*). In fact, one finds $\varpi_k - \varpi_l - \varpi_m = a(k-l-m+\frac{1}{4}+\varepsilon)$ with ε strictly within the interval $(-\frac{1}{4}, \frac{3}{4})$ and $\varpi_k - \varpi_l - \varpi_m - \varpi_n = a(k-l-m-n+\frac{1}{2}+\varepsilon)$ with ε strictly within $(-\frac{1}{2}, \frac{1}{2})$, by straightforward estimation of the second and third term in (3.34) using $k \geqslant 2$ and $l, m, n \geqslant 1$. Because k, l, m and n are integer, this implies that neither $\varpi_k - \varpi_l - \varpi_m$ nor $\varpi_k - \varpi_l - \varpi_m - \varpi_n$ can be zero.

Proving $\varpi_k - \varpi_l - \varpi_m + \varpi_n = 0$ only if $k = l$ and $m = n$ is more difficult. A simple argument based on an estimate as for the other cases cannot be sufficient because this would rule out the trivial resonances, which we know to exist, as well. In order to exclude the non-trivial resonances, the fact that $k > l$ must play a role in the proof. It is given in the Appendix.

The friction coefficient c_k in (3.28) is proportional to the empirical value r. The dependence on the mode number k is determined by the interaction integral $\mathscr{R}_{k,k} = \int_0^1 u_k^* u_k \, \mathrm{d}x$. The calculations yield

$$\mathscr{R}_{k,k} = \tfrac{1}{2}, \qquad \text{for constant depth,} \tag{3.35a}$$

$$\mathscr{R}_{k,k} = \frac{1 - J_1{}^2(p_k)}{2J_1{}^2(p_k)}, \qquad \text{for constant slope,} \tag{3.35b}$$

$$\mathscr{R}_{k,k} = k - \tfrac{1}{4}, \qquad \text{for the quadratically sloping bottom.} \tag{3.35c}$$

$\mathscr{R}_{k,k}$ is constant for the basin with vertical sidewalls, but increases to infinity for $k \to \infty$ in the other two cases.

In order to calculate the coefficients $\Gamma_{k,m}$, the interaction integrals

$$_k\mathscr{C}_{l,m} = \int_0^1 \gamma \zeta_k^* \frac{\mathrm{d}}{\mathrm{d}x}[\zeta_l u_m] \, \mathrm{d}x,$$

$$_k\mathscr{A}_{l,m} = \int_0^1 D^{(0)} u_k^* u_l \frac{\mathrm{d}u_m}{\mathrm{d}x} \, \mathrm{d}x,$$

the one-dimensional equivalents of (3.17), must be evaluated. For this purpose the software packages Maple and *Mathematica* were used. In the case of constant water depth, the integrals can be evaluated analytically. These packages even managed to obtain an (elaborate) analytical expression for the Landau coefficients $\Gamma_{k,m}$. The first four values of the coefficients are $\Gamma_{1,1} = -9.57$, $\Gamma_{1,2} = -12.01$, $\Gamma_{2,1} = -16.79$ and $\Gamma_{2,2} = -16.11$. We have already found that the third-order non-resonance condition (3.12*d*) is not fulfilled for this basin. Although this implies that additional terms, not proportional to $|A_m|^2 A_k$, arise in the amplitude equation (3.28) (cf. (3.27)), these $\Gamma_{k,m}$ are the proper coefficients in front of the $|A_m|^2 A_k$-term.

In the cases of a linear or quadratic bottom profile, the corresponding integrals had to be evaluated numerically. Consequently the infinite sum over n in (3.29), defining $\Gamma_{k,m}$, has to be truncated. The results are shown in figures 3(*a*) and 3(*c*) as a function of the truncation number N. The convergence is quite slow and seems to be alternatingly too low and too high. On plotting the variations on a doubly logarithmic scale they appear to converge at a rate $1/\sqrt{N}$, which might be expected from the fact that this generally is the rate of convergence in a Galerkin expansion.

https://doi.org/10.1017/S0022112004001223 Published online by Cambridge University Press

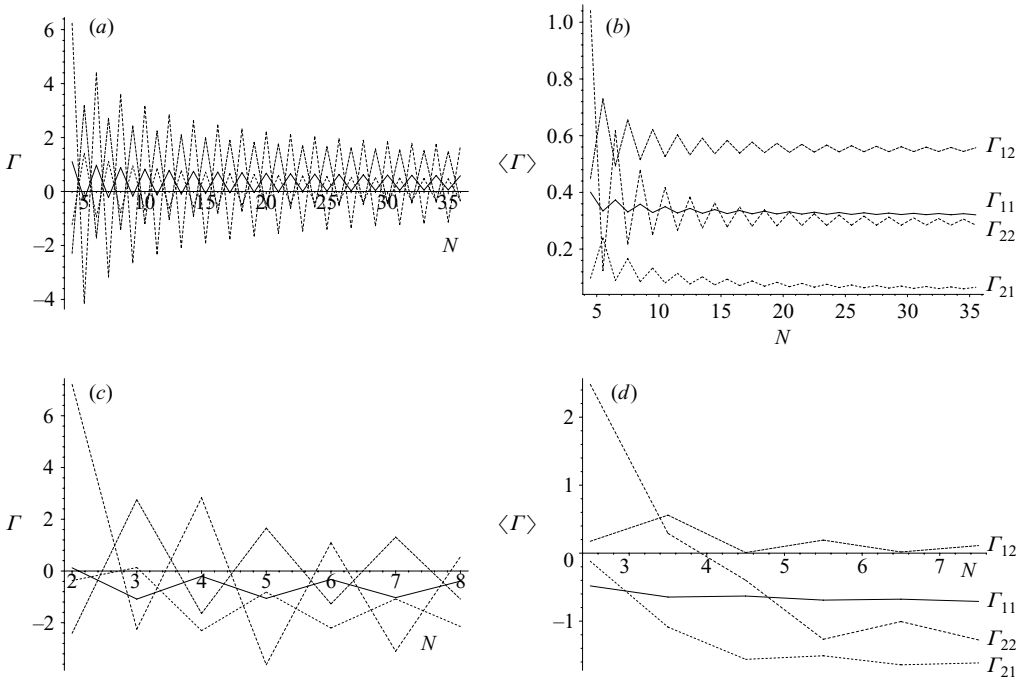


FIGURE 3. Numerical estimation of the interaction coefficients $\Gamma_{k,m}$ for $(k,m)=(1,1)$, $(1,2)$, $(2,1)$ and $(2,2)$. The sum of terms in (3.29) are shown as a function of truncation number N in (a) for the linear bottom and (c) the quadratic bottom. Because of the oscillatory nature of the convergence, subsequent outcomes are averaged in (b) and (d).

The convergence can be improved by taking the average between two subsequent values. Those averages are shown in figures 3(b) and 3(d).

4. Analysis of the Landau equations

In this section, the behaviour of the dynamical system determined by (3.28) will be investigated. For different basins, different values for the coefficients $\mathscr{R}_{k,k}$ and $\Gamma_{k,m}$ will be found, see § 3.4. Therefore the idea is not to consider the problem for specific values of the coefficients, but to study it for arbitrary values in general. Equations similar to (3.28) have been studied by Nayfeh & Mook (1979), but only up to the point of steady states. Multiple equilibria are found by them as well, but chaotic dynamics are beyond the scope of that book.

Neglecting the Coriolis force leads to real-valued coefficients $\Gamma_{k,m}$. In that case, the equations have some symmetry (that disapppears again with the introduction of the Earth's rotation). Therefore, (3.28) will be considered first for real-valued coefficients $\Gamma_{k,m}$. The effects of the Earth's rotation will be investigated later.

4.1. *Boundedness and truncation*

The forcing terms $F_k(\tau)$ in (3.28) are essentially the amplitudes of the components of the external tide with frequency near ω_k. They form the (generalized) Fourier components of the exterior tidal curve with respect to the eigenfrequencies ω_k. It follows from Fourier theory that these amplitudes will be bounded. Moreover, they tend to zero for $\omega_k \to \infty$, and hence for $k \to \infty$.

https://doi.org/10.1017/S0022112004001223 Published online by Cambridge University Press

The Landau equation (3.28) is an equation for the slow evolution of the complex amplitudes A_k. Hence, for each k it amounts to two equations for two unknowns in real coordinates. In order to state the equations in polar coordinates the modulus and argument of the amplitudes are introduced: $A_k = R_k e^{i\Phi_k}$ and $F_k = Z_k e^{i\Psi_k}$. In these coordinates (3.28) become

$$\frac{dR_k}{d\tau} = -c_k R_k + Z_k \cos(\Psi_k - \Phi_k), \tag{4.1a}$$

$$R_k \frac{d\Phi_k}{d\tau} = \sum_m \Gamma_{k,m} {R_m}^2 R_k + Z_k \sin(\Psi_k - \Phi_k). \tag{4.1b}$$

From the radial equation (4.1*a*) it is clear that the amplitude R_k decreases if $R_k > Z_k/c_k$. We conclude that $|A_k| \leqslant Z_k/c_k$ for $\tau \to \infty$. The estimate $|A_k| \leqslant Z_k/c_k$ ensures that the (absolute) convergence of the response amplitudes A_k follows from the convergence of the forcing amplitudes Z_k. If a certain mode k is not excited by the external tide ($Z_k = 0$) then it is not excited by other modes either. In particular for harmonic forcing, if the exterior tide ζ_e consists of a single tidal constituent, then Z_k is non-zero, hence A_k is as well, for a single component k only. Because the amplitudes Z_k of the tidal harmonics ultimately decrease with increasing frequency, it makes sense to truncate the model and consider (3.28) for a finite number of modes. This will be done in §§ 4.2, 4.3.

Note that the form of (4.1*a*) depends on the assumption that $\Gamma_{k,m}$ is real, and hence on neglecting the Earth's rotation. For complex-valued $\Gamma_{k,m}$ there is a contribution of the nonlinear terms in the radial equation as well. This invalidates the preceding argument. In combination with the Earth's rotation the nonlinear effects of continuity and advection can cause growth of the solution's amplitudes. For real-valued $\Gamma_{k,m}$ the interaction between modes is not present in the radial equations. The interaction between the modes is entirely through the phases Φ_k.

4.2. *Single-mode solution*

In this section, the external tide is assumed to be in effective resonance with only one eigenmode of the basin, hence $F_k \neq 0$ for one k only. According to the reasoning in the previous section, the dynamics will be dominated by this single resonant eigenmode k; all other modes will be negligible. The (complex) amplitude A_k of this mode is governed by

$$\frac{dA_k}{d\tau} = F_k(\tau) - c_k A_k + i \Gamma_{k,k} |A_k|^2 A_k,$$

which is just the truncation of (3.28) to a single mode. In this section the connection with previous work by Doelman *et al.* (2002) will be established first. Consequently an overview of the results of their analysis is given: the determination of stationary states, yielding multiple equilibria, mechanisms leading to chaotic dynamics and the construction of a chaotic set for one of those mechanisms are discussed.

If the external tide is in perfect resonance with eigenmode k, i.e. $\zeta_e \sim e^{i\omega_k t}$, then $F_k(\tau)$ is a constant, related to the amplitude of the tidal signal. A more natural situation is the case of near resonance, when the temporal behaviour of the external tidal component is $e^{i\omega t}$, where the forcing frequency $\omega = \omega_k + \alpha^2\sigma$ deviates slightly ($O(\alpha^2)$ only for the modulation to be on the same time scale as the evolution due to the nonlinear effects) from the eigenfrequency ω_k. In this case one has $e^{i\omega t} = e^{i\omega_k t} e^{i\sigma\alpha^2 t} = e^{i\sigma\tau} e^{i\omega_k t}$ from which it follows that $F_k(\tau)$ is proportional to $e^{i\sigma\tau}$, say $F_k(\tau) = Z e^{i(\sigma\tau + \Psi)}$. It is convenient to write $A_k(\tau) = A(\tau) e^{i\sigma\tau}$, which introduces an additional term $-i\sigma A$ in the amplitude

https://doi.org/10.1017/S0022112004001223 Published online by Cambridge University Press

equation. Suppressing the subscript k, this leads to

$$\frac{\mathrm{d}A}{\mathrm{d}\tau} = -(c+\mathrm{i}\sigma)A + \mathrm{i}\,\Gamma\,|A|^2A + Z\mathrm{e}^{\mathrm{i}\Psi}, \tag{4.2}$$

which in polar coordinates $A = R\mathrm{e}^{\mathrm{i}\Phi}$ becomes

$$\frac{\mathrm{d}R}{\mathrm{d}\tau} = -c\,R + Z\cos(\Psi-\Phi), \tag{4.3a}$$

$$R\frac{\mathrm{d}\Phi}{\mathrm{d}\tau} = -\sigma R + \Gamma R^3 + Z\sin(\Psi-\Phi), \tag{4.3b}$$

and in Cartesian coordinates $A = X + \mathrm{i}Y$

$$\frac{\mathrm{d}X}{\mathrm{d}\tau} = (\sigma-\Gamma R^2)Y - cX + Z\cos(\Psi), \tag{4.4a}$$

$$\frac{\mathrm{d}Y}{\mathrm{d}\tau} = -(\sigma-\Gamma R^2)X - cY + Z\sin(\Psi), \tag{4.4b}$$

with $R^2 = X^2 + Y^2$. In this form the equations are completely equivalent to the ones studied in Maas (1997), Maas & Doelman (2002) and Doelman *et al.* (2002).† In those papers, the equations were derived by averaging methods in a zero-dimensional model for so-called Helmholtz oscillators, see § 1. Averaging is another way to describe the slow behaviour of the model. The results are equivalent: an equation for the slow evolution of the amplitudes of oscillations on the fast time scale. Because equations (4.3) and (4.4) are essentially the same as the ones found in Maas & Doelman (2002) and Doelman *et al.* (2002), their results apply here as well. Those results will only be summarized here, for details refer to the original papers. Note that, although the form of the amplitude equations is essentially the same, the difference between them lies in the fact that the equations were derived for a much larger class of basins in the present paper. The restriction to almost-enclosed Helmholtz-resonators was lifted in this study.

The system exhibits stationary solutions. They correspond to a response of the system at the same frequency as the forcing and with constant amplitude. From (4.2) one can derive the amplitude response equation, describing the response amplitude R as a function of the forcing frequency σ and amplitude Z. However, it is much easier to give the frequency σ in terms of Z and R, which yields

$$\sigma = \Gamma R^2 \pm \frac{Z}{R}\sqrt{1-\left(\frac{cR}{Z}\right)^2} \tag{4.5}$$

The resulting response curve is plotted in figure 4, for three values of the forcing amplitude Z. It clearly shows the effect of the nonlinear terms in bending the resonance horn because the effective eigenfrequency now depends on the response amplitude. In linear theory one would find a single response amplitude for each value of the frequency σ. In this case however, it is possible to find multiple stationary solutions. It appears that, if there are three response solutions for given parameters σ and Z, the response with largest and the response with smallest amplitude are stable. The 'medium amplitude response' is an unstable solution of (4.2), represented in figure 4

† Compare (4.3) and (4.4) with respectively (3.6) and (3.8) in Doelman *et al.* (2002), where $F_{sol} = 0$ here.

https://doi.org/10.1017/S0022112004001223 Published online by Cambridge University Press

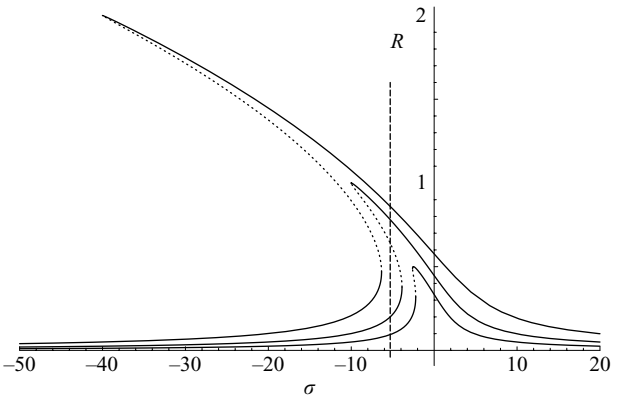


FIGURE 4. Frequency response curves for $\Gamma = -10$, $c = 1$ and several forcing amplitudes, $Z = \frac{1}{2}, 1, 2$. Solid curves denote stable branches, the dotted curves are unstable. A vertical line at $\sigma = -5.3$ indicates that multiple equilibria are found under certain conditions.

by a dotted line. This means that under those external conditions, the system can be found in either an amplified or a choked tidal regime, depending on the history of the system.

Under slow changes of external conditions, like mean sea-level rise or changing morphology, the system will follow one of the stable branches. However, if such a branch 'folds', hence ceases to exist, the system will make a sudden transition to the remaining stable branch if the external conditions change further. If the parameters change very slowly, the system will have time to settle down to the new regime. If however the parameters change back and forth before the system has time to reach the corresponding stationary states, the reaction of the system can be chaotic, as will be discussed below. There are two obvious ways in which the forcing parameters σ (frequency) and Z (amplitude) can be changed on the time scale τ of the transient amplitude behaviour in (4.2): either a slow change in water depth or forcing amplitude modulations, the latter due to e.g. the spring-neap tidal cycle. In relatively small basins, a slow change in water depth could be due to large-scale tidal motion, with the resonant eigenmode representing secondary undulations on a much smaller time scale. It constitutes a slow change in the basin's characteristics, and hence its eigenfrequency. This effectively amounts to changing the forcing frequency σ relative to the eigenfrequency, see Maas & Doelman (2002, § 5). The analysis in this paper does not capture this process accurately, although it is in principle possible to incorporate this effect in the present model as well.

In the case of amplitude modulations a so-called 'horseshoe' has been found as a subsystem of the model under some additional assumptions, thus constituting a proof of the occurrence of chaos in the system (Doelman *et al.* 2002). This construction will be illustrated here. The external forcing is assumed now to consist of two tidal components, one much smaller in amplitude than the other, and both almost in resonance with the one eigenfrequency ω_k, as is appropriate for many areas where the tidal signal is dominated by the lunar M_2-tidal component, with a small modulation due to the solar S_2-constituent. As explained for one tidal component at the beginning of this section, this leads to $F_k(\tau) = Z_1 e^{i(\sigma_1 \tau + \Psi_1)} + Z_2 e^{i(\sigma_2 \tau + \Psi_2)}$. The

https://doi.org/10.1017/S0022112004001223 Published online by Cambridge University Press

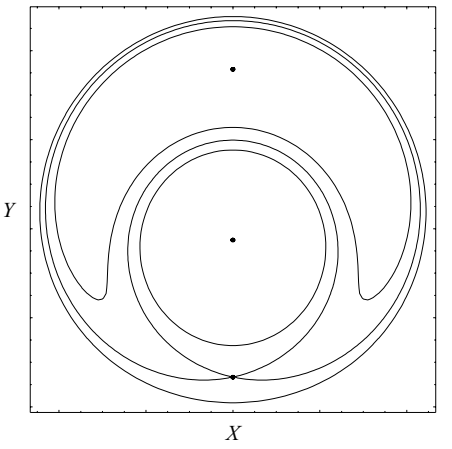


FIGURE 5. Phase portrait of Hamiltonian flow for $Z_1 = \frac{1}{24}\sqrt{3}$. This choice for Z_1 is arbitrary. When $0 < Z_1 < \frac{2}{9}\sqrt{3}$, there are three stationary states and the result is similar.

assumption formulated above can be written $Z_2/Z_1 = \delta$, with $\delta \ll 1$, which leads to

$$\begin{aligned} F_k(\tau) &= Z_1 e^{i(\sigma_1 \tau + \Psi_1)} + Z_2 e^{i(\sigma_2 \tau + \Psi_2)} \\ &= Z_1 e^{i(\sigma_1 \tau + \Psi_1)} \left(1 + \delta e^{i(\Delta\sigma\, \tau + \Delta\Psi)}\right) \\ &= Z(\tau) e^{i(\sigma \tau + \Psi(\tau))}, \end{aligned}$$

where $\sigma = \sigma_1$, $\Delta\sigma = \sigma_2 - \sigma_1$, $\Delta\Psi = \Psi_2 - \Psi_1$, $Z(\tau) = Z_1(1 + \delta\cos(\Delta\sigma\, \tau + \Delta\Psi)) + O(\delta^2)$, and $\Psi(\tau) = \Psi_1 + \delta\sin(\Delta\sigma\, \tau + \Delta\Psi) + O(\delta^2)$. The expression for $F_k(\tau)$ is similar to that for a single tidal component. Therefore, (4.2), (4.3) and (4.4) are equally valid, with the only difference that Z and Ψ depend on τ now. Moreover, in conjunction with assuming small modulation, friction is assumed to be additionally small as well, by written $c = \delta C$. By rescaling, the system is brought into the form

$$\frac{dX}{d\tau} = (1 - R^2)Y + Z_1 + \delta[-CX + Z_1 \sin(\Delta\sigma\, \tau)], \tag{4.6a}$$

$$\frac{dY}{d\tau} = -(1 - R^2)X + \delta[-CY - Z_1 \cos(\Delta\sigma\, \tau)], \tag{4.6b}$$

which is the same as (3.16) in Doelman *et al.* (2002) except for interchanging X and Y.

System (4.6) is Hamiltonian for $\delta = 0$; the Hamiltonian is given by

$$\mathscr{H}(X, Y) = -\tfrac{1}{4}(1 - R^2)^2 + Z_1 Y. \tag{4.7}$$

The resulting phase portrait is shown in figure 5 under conditions for which there are multiple equilibria. One of the critical points is a saddle, the other two are centre points. The saddle corresponds to the unstable stationary solution from figure 4. The centres correspond to the stable stationary solutions in figure 4. The 'inner' one is the choked mode with small amplitude, the 'outer' one is the amplified mode with an amplitude which is larger than the amplitude of the saddle. Two homoclinic orbits are connected to the saddle.

For $\delta \neq 0$ the system (4.6) is not autonomous, so the phase portrait in figure 5 is not appropriate anymore. For small $\delta \ll 1$ it can be used as a first approximation however. The persistence of the homoclinic orbits can be investigated using the Melnikov method. In fact, the deviation from the unperturbed homoclinic orbit in

https://doi.org/10.1017/S0022112004001223 Published online by Cambridge University Press

figure 5 is approximated by calculating the approximative change of the Hamiltonian $\mathscr{H}$ due to the $O(\delta)$ perturbations by friction and modulation. This determines if they are connected still, or if the stable and unstable manifolds of the saddle point — the points that tend to respectively come from it — do not meet and spiral down to the critical points. The analysis by Doelman *et al.* (2002) shows that the stable and unstable manifolds do intersect transversely if friction is not too large (for $C < C_{max}(Z_1, \Delta\sigma)$). Note that transverse intersections between stable and unstable manifolds are possible due to the non-autonomous nature of (4.6). In that case the well-known 'horseshoe' can be constructed (the Smale-Birkhoff theorem), which yields a chaotic set, consisting of chaotic orbits which evolve close to the homoclinic orbits of figure 5 again and again in an irregular way. The physical consequence is that harmonic 'constants' cannot be found because they evolve chaotically on longer time scales (cf. Doodson 1924; Gutiérrez *et al.* 1981).

A final remark should be made about the value of the parameter δ. It must be small in order for the Melnikov method to be applicable. The parameter α should be even smaller, to maintain the validity of the amplitude equation (4.2). However, though this assumption on δ is needed to construct the horseshoe map by the Melnikov method, the smallness of δ, i.e. of the modulation of the external forcing, is likely not to be required at all. It is to be expected that for larger δ, chaotic motion still occurs. This is motivated for example by the numerical observations in Maas (1997) and Maas & Doelman (2002).

4.3. *Two-mode solutions*

In order to investigate the influence of one mode on the other, it is natural to consider the model with two modes. Hence, in this section the external forcing is assumed to be in resonance with two eigenmodes of the basin. Without loss of generality we call them mode 1 and mode 2, referring to these modes by means of corresponding indices. The external forcing will give rise to $F_k = Z_k e^{i(\sigma_k \tau + \Psi_k)}$, for $k = 1, 2$. Continuing as in the previous section, we replace $A_k(\tau)$ by $A_k e^{i\sigma_k \tau}$ resulting in the equations

$$\frac{dA_1}{d\tau} = -c_1 A_1 - i\sigma_1 A_1 + i(\Gamma_{1,1}\,|A_1|^2 + \Gamma_{1,2}\,|A_2|^2)A_1 + Z_1 e^{i\Psi_1}, \tag{4.8a}$$

$$\frac{dA_2}{d\tau} = -c_2 A_2 - i\sigma_2 A_2 + i(\Gamma_{2,1}\,|A_1|^2 + \Gamma_{2,2}\,|A_2|^2)A_2 + Z_2 e^{i\Psi_2}. \tag{4.8b}$$

In polar coordinates $A_k = R_k e^{i\Phi_k}$ we have

$$\frac{dR_1}{d\tau} = -c_1 R_1 + Z_1 \cos(\Psi_1 - \Phi_1), \tag{4.9a}$$

$$R_1 \frac{d\Phi_1}{d\tau} = -\left(\sigma_1 - \Gamma_{1,1} R_1^2 - \Gamma_{1,2} R_2^2\right) R_1 + Z_1 \sin(\Psi_1 - \Phi_1), \tag{4.9b}$$

$$\frac{dR_2}{d\tau} = -c_2 R_2 + Z_2 \cos(\Psi_2 - \Phi_2), \tag{4.9c}$$

$$R_2 \frac{d\Phi_2}{d\tau} = -\left(\sigma_2 - \Gamma_{2,1} R_1^2 - \Gamma_{2,2} R_2^2\right) R_2 + Z_2 \sin(\Psi_2 - \Phi_2). \tag{4.9d}$$

The next subsection deals with the stationary solutions of these equations which can be studied analytically. Figure 6 shows the four-dimensional response graphs of the response amplitudes R_1 and R_2 as a function of the forcing frequencies σ_1 and σ_2 for fixed forcing amplitudes Z_1 and Z_2. In order to clarify this figure, a classification

https://doi.org/10.1017/S0022112004001223 Published online by Cambridge University Press

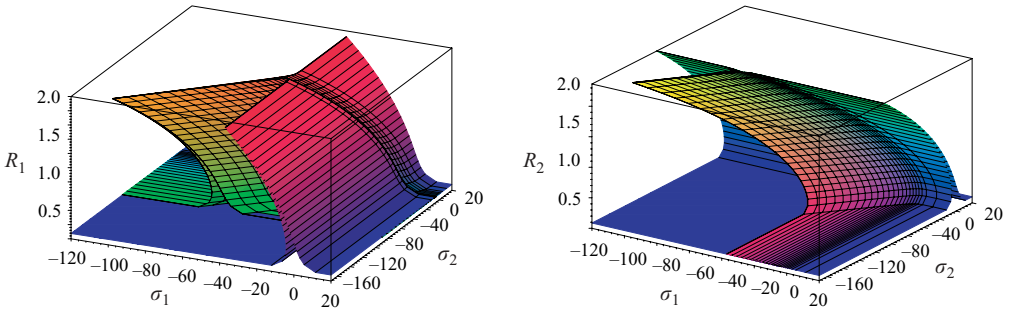


FIGURE 6. For caption see facing page.

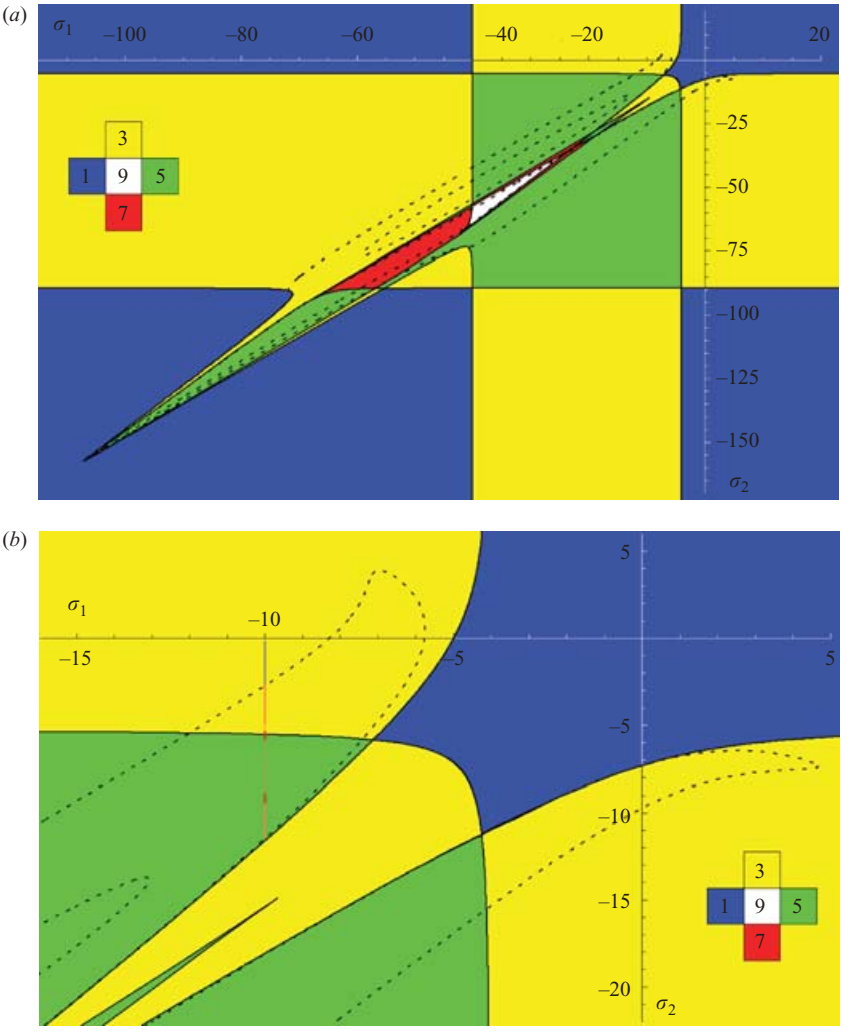


FIGURE 7. For caption see facing page.

https://doi.org/10.1017/S0022112004001223 Published online by Cambridge University Press

of (σ_1, σ_2) parameter space is given in figure 7. The stability of the stationary states is discussed here as well. Moreover, cross-sections of the graphs in figure 6 are shown in figure 8. Finally, the section ends with numerical investigations of the system, showing periodic orbits, period doublings and chaos.

Note that the behaviour described here is that of the amplitudes themselves. The resulting water-level variations will be oscillations with frequencies ω_1, ω_2 of the respective eigenmodes, but with amplitudes and phases modulating slowly in time, according to the dynamics described here. This behaviour would manifest itself if one performs a harmonic analysis on tidal signals over moving windows in time. Instead of being constant over all time frames, the amplitudes and phases found for a tidal component would vary slowly in time. It is this variation of the amplitudes and phases that is studied here.

4.3.1. *Analytical results*

Stationary solutions to these equations correspond again to the response of the system at the same frequencies as the forcing. They follow by equating the derivatives in (4.9) to zero and elimating the angle coordinates. This leads to

$$\sigma_1 = \Gamma_{1,1} {R_1}^2 + \Gamma_{1,2} {R_2}^2 \pm \sqrt{\frac{{Z_1}^2}{{R_1}^2} - {c_1}^2}, \tag{4.10a}$$

$$\sigma_2 = \Gamma_{2,1} {R_1}^2 + \Gamma_{2,2} {R_2}^2 \pm \sqrt{\frac{{Z_2}^2}{{R_2}^2} - {c_2}^2}. \tag{4.10b}$$

Compare this with (4.5) for one mode. For each mode, the response curve R_k as a function of σ_k would be just a shifted copy of figure 4, if the other mode's amplitude were constant. Obviously R_1 depends on σ_1 but it depends on σ_2 as well through the interaction with R_2. The influence of one mode on the other is to change its effective eigenfrequency. Because the shift depends on the amplitude, the result can nevertheless be quite complicated. As in the case of one mode, it is much harder to find the response amplitudes R_1 and R_2 as a function of the detuning frequencies σ_1, σ_2. However, by plotting the frequencies as a function of the amplitudes, one can still parametrically describe the response-'curves'. Figure 6 shows the results. The plots are made with coefficients $\Gamma_{k,m}$ according to the first two eigenmodes of a rectangular

FIGURE 6. The response amplitudes R_1 and R_2 as a function of forcing frequencies. Bay parameters are chosen in accordance with the first two modes of a rectangular basin ($c_1 = c_2 = \frac{1}{2}$, $\Gamma_{1,1} = -10$, $\Gamma_{1,2} = -12$, $\Gamma_{2,1} = -17$, $\Gamma_{2,2} = -16$). The choice $(Z_1, Z_2) = (1, 13/11)$ of forcing amplitudes is arbitrary. Other choices lead to different but similar pictures. The surfaces are parameterized by R_1 and R_2; the black gridlines are for constant R_1 and R_2 respectively. Corresponding branches are in the same colour in both figures: along the blue branches both R_1 and R_2 are small, red is for R_1 finite and small R_2, green denotes small R_1 and finite R_2, orange/yellow branches have both R_1 and R_2 finite.

FIGURE 7. Bifurcation lines in (σ_1, σ_2) parameter space for $Z_1 = 1$, $Z_2 = \frac{13}{11}$, bay parameters as in figure 6. Solid lines mark saddle-node bifurcations and divide the space into regions with a different number of steady states (regions are colour-coded). Dashed lines represent Hopf bifurcations. (*b*) A Zoom of the part of parameter space for which numerical experiments were performed, along the indicated line for $\sigma_1 = -10$.

https://doi.org/10.1017/S0022112004001223 Published online by Cambridge University Press

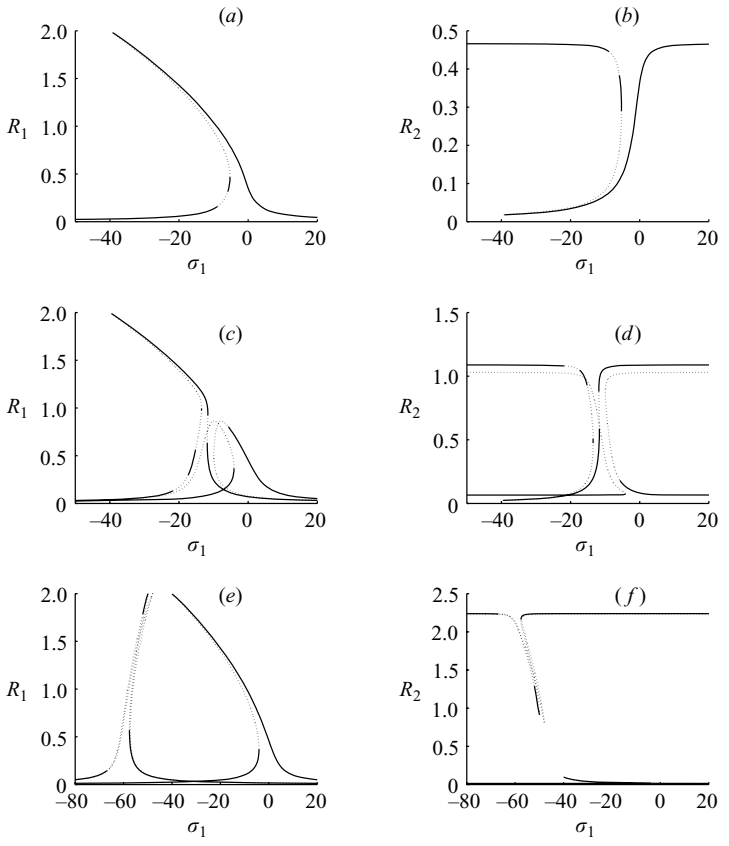


FIGURE 8(a–f). For caption see facing page.

basin with vertical sidewalls, i.e. $\Gamma_{1,1} = -10$, $\Gamma_{1,2} = -12$, $\Gamma_{2,1} = -17$, $\Gamma_{2,2} = -16$ and friction $c_1 = c_2 = \frac{1}{2}$, see § 3.4. Cross-sections, shown in figure 8, will be described later.

Because the response amplitudes depend on both frequencies σ_1 and σ_2, the graphs are three-dimensional. In fact, they should be considered together as four-dimensional graphs of (R_1, R_2) as a function of (σ_1, σ_2). For a given pair of frequencies (σ_1, σ_2) a stationary state is characterized by a pair of amplitudes (R_1, R_2). These states constitute the branches in figure 6; the graphs are not independent from each other. The number of stationary states at given frequencies can be read off from the colours in figure 7. The solid lines in this figure mark the frequency values for which saddle-node bifurcations occur, where two steady states appear or vanish. They are obtained by considering the Jacobian of (4.9):

$$\begin{pmatrix} -c_1 & Z_1 \sin(\Psi_1 - \Phi_1) & 0 & 0 \\ 2\Gamma_{1,1}R_1 - \dfrac{Z_1 \sin(\Psi_1 - \Phi_1)}{{R_1}^2} & -\dfrac{Z_1 \cos(\Psi_1 - \Phi_1)}{R_1} & 2\Gamma_{1,2}R_2 & 0 \\ 0 & 0 & -c_2 & Z_2 \sin(\Psi_2 - \Phi_2) \\ 2\Gamma_{2,1}R_1 & 0 & 2\Gamma_{2,2}R_2 - \dfrac{Z_2 \sin(\Psi_2 - \Phi_2)}{{R_2}^2} & -\dfrac{Z_2 \cos(\Psi_2 - \Phi_2)}{R_2} \end{pmatrix}. \tag{4.11}$$

Using the fact that $Z_k \cos(\Psi_k - \Phi_k) = c_k R_k$, for $k = 1, 2$, in steady states, the Jacobian can be conveniently expressed in terms of the two variables $t_k = \tan(\Psi_k - \Phi_k)$. The

https://doi.org/10.1017/S0022112004001223 Published online by Cambridge University Press

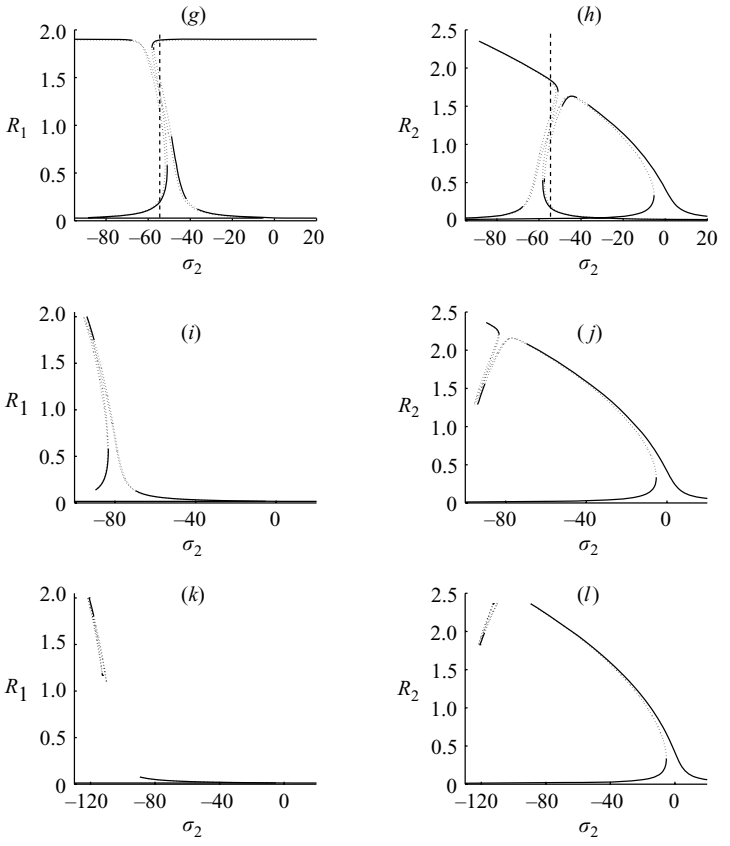


FIGURE 8. Several cross-sections of the response surfaces from figure 6, for the same bay parameters and forcing amplitudes as in the previous figures. (*a–f*)The response amplitudes R_1 and R_2 as a function of σ_1 for (a,b) $\sigma_2 = 1$, (c,d) $\sigma_2 = -18$; (e,f) $\sigma_2 = -80$; $(g–l)$ R_1 and R_2 as a function of σ_2 for (g,h) $\sigma_1 = -36$, (i,j) $\sigma_1 = -60$, (k,l) $\sigma_1 = -80$. The dashed line at $\sigma_2 = -54.5$ in (g) and (h) indicates conditions for which nine different equilibria exist.

characteristic polynomial of (4.11) is

$$p(\lambda) = \lambda^4 + a\lambda^3 + b\lambda^2 + c\lambda + d,$$

where

$$\left.\begin{aligned} a &= 2(c_1 + c_2),\\ b &= 4c_1c_2 + c_1^2\left(1+t_1^2\right) + 2c_1\Gamma_{1,1}R_1^2t_1 + c_2^2\left(1+t_2^2\right) + 2c_2\Gamma_{2,2}R_2^2t_2,\\ c &= 2c_2\left(c_1^2\left(1+t_1^2\right) + 2c_1\Gamma_{1,1}R_1^2t_1\right) + 2c_1\left(c_2^2(1+t_2^2) + 2c_2\Gamma_{2,2}R_2^2t_2\right),\\ d &= \left(c_1^2\left(1+t_1^2\right) + 2c_1\Gamma_{1,1}R_1^2t_1\right)\left(c_2^2\left(1+t_2^2\right) + 2c_2\Gamma_{2,2}R_2^2t_2\right) - 4c_1c_2\Gamma_{1,2}\Gamma_{2,1}R_1^2t_1R_2^2t_2, \end{aligned}\right\} \tag{4.12}$$

with $R_k = Z_k/(c_k\sqrt{1+t_k^2})$. Saddle-node bifurcations occur when $\lambda = 0$ is a root. Solving $d = 0$ for t_2 hence leads to a parametric description of the solid bifurcation lines in figure 7 in terms of t_1.

The stability of the steady states in figure 6 can also change due to Hopf bifurcations. These occur if $\lambda = \mathrm{i}\omega$, with $\omega \in \mathbb{R}$, is a root of $p(\lambda)$, i.e. $\omega^4 - b\omega^2 + d - \mathrm{i}a\omega^3 + \mathrm{i}c\omega = 0$. From the imaginary part $c\omega - a\omega^3$ we find that either $\omega = 0$, resulting in the saddle-node bifurcations already considered, or $\omega^2 = c/a$, which subsequently can be

https://doi.org/10.1017/S0022112004001223 Published online by Cambridge University Press

substituted in the real part of $p(\lambda)$. Solving the resulting condition $c^2 - abc + a^2 d = 0$ leads to a parametrization of the dashed bifurcation lines that are also shown in figure 7. At those values for the frequencies σ_1 and σ_2, one of the branches of steady states undergoes a Hopf bifurcation, generically giving birth to a periodic solution.

Three basic components can be distinguished in figure 6. First one has the steady states with R_1 finite and R_2 very small, or with R_1 very small and R_2 finite. In the first case, because R_2 is negligible, the corresponding frequency σ_2 has hardly any influence on these states. This results in a graph parallel to the σ_2-axis, with constant cross-section perpendicular to that axis, following the one-mode response curve R_1 versus σ_1 (figure 4). The same holds, mutatis mutandis, for the steady states with R_1 very small. Besides those two branches, there are new equilibria with both R_1 and R_2 finite, to be called *two-mode equilibria*. The backbone of these equilibria is described by $\sigma_1 = \Gamma_{1,1} R_1^2 + \Gamma_{1,2} R_2^2$ and $\sigma_2 = \Gamma_{2,1} R_1^2 + \Gamma_{2,2} R_2^2$, for $0 \leqslant R_k \leqslant Z_k/c_k$. Hence this 'backbone' exists in a parallelogram in (σ_1, σ_2) frequency space. The square roots in (4.10) cause the steady states to deviate from it, but the (distorted) parallelogram is still recognizable as such in figure 7(*a*).

Several cross-sections of figure 6 are shown in figure 8. They are obtained using another parameterization of the response-surfaces. In fact, by solving (4.10*a*) with respect to R_2, one can obtain (R_2, σ_2) as a function of (R_1, σ_1). Solving (4.10*b*) for R_1 yields a parameterization of (R_1, σ_1) as a function of (R_2, σ_2). The former can be used to plot intersections for constant σ_1 by choosing a judicious range of values for R_1, the latter for intersections with σ_2 constant. The stability of the respective steady states was determined by calculating the eigenvalues of the Jacobian (4.11). Solid lines indicate stable equilibria, unstable branches are dashed.

The common feature in these cross-sections (for fixed σ_k) is the one-mode response curve when one mode (R_k) is very small. Its stability generally corresponds to that of the one-mode solution, the higher and lower modes being stable and the 'medium amplitude mode' unstable. In figure 8(*a*) (with corresponding figure 8*b*) the lower mode is unstable due to a Hopf bifurcation over a small interval of σ_1-values, apparently due to the influence of the second mode. The new two-mode equilibria are separated from the one-mode response curve in figures 8(*k*), 8(*l*) for $\sigma_1 = -80$. In figures 8(*e*), 8(*f*) the two-mode equilibria are disconnected from the one-mode response curve for R_1 as well. The fact that these branches extend to $\sigma_1 \to \pm\infty$ reflects that the branches are connected with the one-mode solutions for which R_1 is very small. In the other figures the two-mode equilibria and the one-mode response curves are connected. Although they often are unstable, which implies that they would not appear in practice, there are conditions for which the new two-mode equilibria are stable, hence observable in principle. They can occur, even though the one-mode response curve shows low-amplitude solutions at those conditions only. The nonlinear interaction between modes allows the basin to resonate at other frequencies than its linear eigenfrequencies. Multiple equilibria occur in the two-mode system as well (see figure 7), with a maximum of nine equilibria under conditions indicated by intersections with the dashed line in figures 8(*g*), 8(*h*).

There is hardly any difference (apart from interchanging R_1 and R_2) between the cross-sections perpendicular to the σ_2-axis and those perpendicular to the σ_1-axis. All figures are shown here for $Z_1 = 1$ and $Z_2 = \frac{13}{11}$. For other choices the differences are similar to those between the cross-sections for constant σ_1 or σ_2. Increasing friction (parameters c_1 and c_2) blurs the picture: the width of the resonance peaks increases, thus obscuring their backbone structure. In particular the bending of the resonance 'curves', hence the multiple equilibria, ultimately disappears.

https://doi.org/10.1017/S0022112004001223 Published online by Cambridge University Press

4.3.2. *Numerical integrations*

Using the numerical dynamical systems package DsTool (Guckenheimer *et al.* 1992), the system (4.8) was investigated near one of the Hopf bifurcations. In fact, some experiments were carried out for $\sigma_1 = -10$ and σ_2 ranging between 0 and -11.5, along the line indicated in figure 7(*b*). There are multiple equilibria under these circumstances, but we focused on one particular branch only, with R_1 being lowest and R_2 highest of three at $\sigma_2 = 0$ (this order is not preserved throughout). Therefore some of the bifurcation lines that are crossed in figure 7(*b*) are not relevant because they occur on other branches. On the selected branch a Hopf bifurcation occurs when the dashed line is crossed. The solid line crossed at $\sigma_2 = -11.6$ marks a saddle-node bifurcation, thus ending this branch. The solid line which is crossed at about $\sigma_2 = -5.2$, marks a saddle-node bifurcation that occurs on another branch.

The stationary state is stable for σ_2 just above the saddle-node bifurcation at $\sigma_2 = -11.6$. On increasing σ_2 from there a supercritical Hopf bifurcation occurs: a stable periodic solution to (4.8) appears for σ_2 just above -11.48. This solution undergoes period doubling at $\sigma_2 = -9.44, -9.42, \ldots$. This orbit is shown in the left-hand column of figure 9 at $\sigma_2 = -9.416$, after two period doublings. The difference betweeen subsequent oscillations is hardly visible in the time series 9(*a*) for the imaginary part Y_1 of the first mode, although the fourfold symmetry breaking is still reasonably distinct in the phase portraits 9(*d*) and 9(*g*). After a cascade of period doublings a chaotic attractor is found, for which the time series for Y_1 and projections of the orbit in phase space are shown for $\sigma_2 = -9.3$. Regime behaviour, a common feature in chaotic systems, is found: the amplitude of the oscillations collapses suddenly and starts to grow again, until at some moment another collapse occurs. Although the growth process seems to behave regularly, the period between two collapses is irregular. The chaotic nature of the motion is corroborated furthermore by the Poincaré section in figures 9(*f*), 9(*i*), showing the return map to the plane $R_1 = 0.4$. A Hénon-like fractal attractor is found.

At $\sigma_2 = -9.29$ the chaotic attractor becomes unstable: orbits starting close to the chaotic set stay close for some time, but ultimately end up at one of the remaining stable fixed points . It remains unstable till $\sigma_2 = -5.61$, above which a stable chaotic attractor is found again. It originates from a cascade of period doublings at $\sigma_2 = -5.00, -5.38, \ldots$ when decreasing σ_2 below the (supercritical) Hopf bifurcation at $\sigma_2 = -2.72$. For $\sigma_2 > -2.72$ the stationary solutions is stable again: no periodic orbit is found anymore.

4.4. *Mechanisms for chaos*

Chaotic behaviour is found in system (3.28), both in § 4.2 for one mode, and in § 4.3 for two modes. The mechanism responsible for the chaos is different however. In this subsection a number of mechanisms that can lead to chaos are discussed. For a system with only one eigenmode, such as an almost-enclosed basin with its corresponding Helmholtz mode (the dynamics of which was discussed by Maas 1997, Maas & Doelman 2002 and Doelman *et al.* 2002) no chaotic behaviour was found if the exterior tide ζ_e is harmonic. Quasi-periodic forcing, i.e. multiple tidal constituents in ζ_e, is necessary to obtain complex dynamics. In the present model however, chaotic behaviour is possible for harmonic forcing as well, due to the possible interaction between eigenmodes. Mechanisms of this kind are discussed in a separate section (§ 4.4.2).

https://doi.org/10.1017/S0022112004001223 Published online by Cambridge University Press

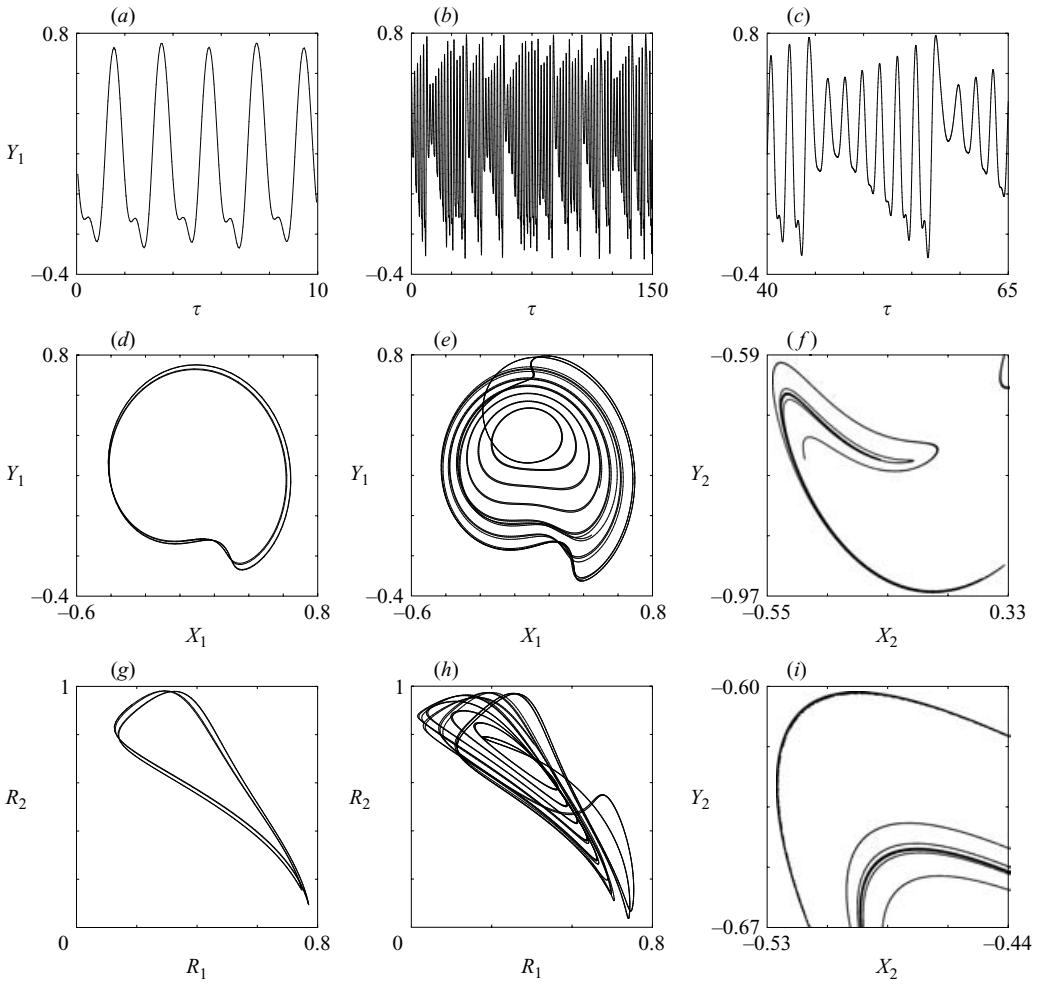


FIGURE 9. Time series and projections of the orbit in phase space for the chaotic attractor at $\sigma_1 = -10, \sigma_2 = -9.3$. The Poincaré section for the return map to the plane $R_1 = 0.4$ is shown in (f) and (i). For comparison, the periodic attractor at $(\sigma_1, \sigma_2) = (-10, -9.416)$, after two period doublings, is shown as well. (a) Time series, $\sigma_2 = -9.416$; (b) time series, $\sigma_2 = -9.3$; (c) zoom of time series; (d) first mode trajectory, $\sigma_2 = -9.416$; (e) first mode trajectory, $\sigma_2 = -9.3$; (f) Poincaré section, lower left section in (X_2, Y_2)-space; (g) amplitudes, $\sigma_2 = -9.416$; (h) amplitudes, $\sigma_2 = -9.3$; (i) upper left part of (f).

4.4.1. *Quasi-periodic forcing*

If two components of the tidal signal ζ_e at sea (for example the M_2- and S_2-components, causing the spring-neap tidal cycle) are nearly in resonance with a single eigenfrequency of the basin, this single mode is forced with slowly modulating forcing amplitude (and phase). As discussed in § 4.2, it was shown in Doelman *et al.* (2002) that this leads to chaotic behaviour of the system. The mechanism stems from the fact that the response curve (4.5) changes with changing forcing amplitude Z. The system has to adapt to a new stable equilibrium when it passes the end of a stable branch. However, before the system has settled to the new regime, the forcing amplitude has changed again, causing continuous regime changes in a chaotic manner. In Maas (1997) this was observed first for a model describing an almost-enclosed basin, with

https://doi.org/10.1017/S0022112004001223 Published online by Cambridge University Press

only one mode, the Helmholtz or pumping mode. In this paper it is shown that those conclusions hold for more general basins as well, if one of its eigenmodes is resonantly forced with two components.

Another mechanism, mentioned already by Maas & Doelman (2002), occurs if the external tide ζ_e consists of one component which is very slow compared to the eigenmodes of the basin and one which is nearly resonant with one of the eigenfrequencies. This might happen for relatively small basins, such as fjords or harbours, with large eigenfrequencies (periods of hours), the 'slow' component being M_2 and an eigenfrequency being resonant with one of its overtones M_{2n} or with another 'high'-frequency component in (the continuum part of) the water-level spectrum (cf. Munk & Cartwright 1966). The slow component of the external tide amounts to a slow change of the reference water depth in the basin. As a consequence its eigenmodes change. For an almost-enclosed basin, where the relatively simple Helmholtz mode is the only eigenmode of interest, determination of the change in eigenfrequency is quite straightforward. Because the frequency σ in (4.5) is relative to the eigenfrequency, this constitutes a slow change of σ. Hence a mechanism similar to the previous case occurs. The system will change between regimes while σ moves along the response curve (4.5). Under appropriate conditions the regime changes will occur in a chaotic manner. In principle this mechanism applies for the model derived in this paper as well. A detailed analysis is more complicated however, because it necessitates calculating the change of the eigenmodes due to a slow change in water depth.

In contrast with previous studies, the model derived in this paper deals with more than one eigenmode. This allows the possibility of two different eigenmodes being resonantly forced by the external tide ζ_e. This situation is discussed in §4.3. With a single tidal component forcing each of the two eigenmodes, the forcing amplitudes Z_1 and Z_2 are constant. In the corresponding case for one mode (§4.2) this leads to multiple equilibria, but no chaos. In the two-mode case however, the behaviour of the sytem can be richer. Periodic orbits for the response amplitudes are found and numerical evidence of chaos has been provided. The interaction between modes is only through the phase equation, where it can be seen as one mode modifying the eigenfrequency of the other. In that respect the mechanism is comparable with the previous one, although the time dependence results from an instability in the interaction between the two modes in this case. Although explicit time dependence of the amplitude equations was needed for the one-mode cases, whereas Z_1 and Z_2 may be constant in the two-mode case for chaos to occur, this is not an essential difference either. For all three mechanisms discussed so far, chaos occurs only if the forcing tide ζ_e at sea comprises at least two components. For the first and third mechanism both need to be in resonance with an eigenmode, either a single one or two different ones. For the second mechanism only one component needs to be resonant; the other component must be slowly evolving on the same time scale at which the system adapts to new equilibria.

The mechanism discussed in the previous paragraph dealt with both amplitudes Z_1 and Z_2 being $O(1)$ (note that this still amounts to small amplitudes at sea due to the scaling of ζ_e compared to ζ). If one forcing component, say Z_2, were even smaller, then the corresponding response amplitude R_2 would be equally small. This situation gives rise to an approximate mathematical approach. For this we assume $Z_2 = \delta z = O(\delta)$ with $\delta \ll 1$. Similar to the analysis in Doelman *et al.* (2002) we assume friction to be additionally small, $c_1 = \delta^2 C_1 = O(\delta^2)$, but $c_2 = O(1)$ may not be small. This is a realistic scenario if mode 1 is one of the first eigenmodes, whereas mode 2

https://doi.org/10.1017/S0022112004001223 Published online by Cambridge University Press

is, although denoted here by the subscript 2, a fairly high eigenmode, because c_k generally increases with k (see § 3.4). This scaling implies that R_2, the amplitude of the second eigenmode, is $O(\delta)$. Hence we write $R_2 = \delta r$, $X_2 = \delta x$ and $Y_2 = \delta y$ to obtain the following amplitude equations in Cartesian coordinates (cf. (4.8)):

$$\frac{\mathrm{d}X_1}{\mathrm{d}\tau} = \left(\sigma_1 - \Gamma_{1,1}R_1^2 - \delta^2\Gamma_{1,2}r^2\right)Y_1 - \delta^2 C_1 X_1 + Z_1\cos(\Psi_1), \tag{4.13a}$$

$$\frac{\mathrm{d}Y_1}{\mathrm{d}\tau} = -\left(\sigma_1 - \Gamma_{1,1}R_1^2 - \delta^2\Gamma_{1,2}r^2\right)X_1 - \delta^2 C_1 Y_1 + Z_1\sin(\Psi_1), \tag{4.13b}$$

$$\frac{\mathrm{d}x}{\mathrm{d}\tau} = \left(\sigma_2 - \Gamma_{2,1}R_1^2 - \delta^2\Gamma_{2,2}r^2\right)y - c_2 x + z\cos(\Psi_2), \tag{4.13c}$$

$$\frac{\mathrm{d}y}{\mathrm{d}\tau} = -\left(\sigma_2 - \Gamma_{2,1}R_1^2 - \delta^2\Gamma_{2,2}r^2\right)x - c_2 y + z\sin(\Psi_2), \tag{4.13d}$$

where ${R_1}^2 = {X_1}^2 + {Y_1}^2$ and $r^2 = x^2 + y^2$. Up to $O(\delta^2)$, the first mode is governed by the Hamiltonian flow with Hamiltonian

$$\mathscr{H}(X, Y) = \frac{-1}{4\Gamma_{1,1}}(\sigma_1 - \Gamma_{1,1}{R_1}^2)^2 + Z_1\cos(\Psi_1)Y_1 - Z_1\sin(\Psi_1)X_1,$$

which is the unscaled variant of (4.7), whereas the equation for the second mode is linear. Hence the phase portrait of the first-order flow for the first mode is known, see Doelman *et al.* (2002). Evolving along one of those periodic or homoclinic orbits, the first mode drives the second parametrically. The second mode couples back to the first mode at $O(\delta^2)$, in a similar way as in the second mechanism discussed before, by modulating the effective eigenfrequency. The modulation by R_2 reflects the first-order behaviour of R_1 in this case. This is the setting in which perturbation theory could be applied, using Melnikov functions to estimate the change of the Hamiltonian, due to friction and the interaction with the second mode, while evolving along the first-order orbits of the one-mode system. One may be able to construct (stable) periodic and homoclinic orbits in the full two-mode system in this way and possibly chaos of the Shilnikov-type (Guckenheimer & Holmes 1983; Wiggins 1988).

4.4.2. *Harmonic forcing*

For all mechanisms described in the previous subsection, the external tide needs to be non-harmonic for chaos to occur. A harmonic external tide ζ_e with one tidal constituent can lead to chaos as well if one mode can excite another. This is possible if Coriolis effects are taken into account. In the context of the present paper, Coriolis forces cause the eigenfunctions of (3.8), (3.9) to be non-real. Physically this means phase differences within the eigenmode over the basin; mathematically it leads to non-real coefficients $\Gamma_{k,m}$. Writing $\Gamma_{k,m} \mapsto \Gamma_{k,m} + \mathrm{i}\Delta_{k,m}$ and $Z_2 = 0$, the equivalent of (4.9) is

$$\frac{\mathrm{d}R_1}{\mathrm{d}\tau} = -\left(c_1 + \Delta_{1,1}R_1^2 + \Delta_{1,2}R_2^2\right)R_1 + Z_1\cos(\Psi_1 - \Phi_1), \tag{4.14a}$$

$$R_1\frac{\mathrm{d}\Phi_1}{\mathrm{d}\tau} = -\left(\sigma_1 - \Gamma_{1,1}R_1^2 - \Gamma_{1,2}R_2^2\right)R_1 + Z_1\sin(\Psi_1 - \Phi_1), \tag{4.14b}$$

$$\frac{\mathrm{d}R_2}{\mathrm{d}\tau} = -\left(c_2 + \Delta_{2,1}R_1^2 + \Delta_{2,2}R_2^2\right)R_2, \tag{4.14c}$$

$$R_2\frac{\mathrm{d}\Phi_2}{\mathrm{d}\tau} = -\left(\sigma_2 - \Gamma_{2,1}R_1^2 - \Gamma_{2,2}R_2^2\right)R_2. \tag{4.14d}$$

https://doi.org/10.1017/S0022112004001223 Published online by Cambridge University Press

The essential difference with the system for real $\Gamma_{k,m}$ is that one mode can now excite others. More specifically, if $\Delta_{2,1} < 0$, the first mode can destabilize the global attractor $R_2 = 0$ to which the second mode would otherwise decay for $Z_2 = 0$. If one of the diagonal elements $\Delta_{k,k}$ is negative, then mode k causes positive feedback to itself and will grow without bound, thus escaping the validity of the present model. In that case higher-order terms should be taken into account. Positive $\Delta_{k,k}$ provide an additional damping mechanism, manifested at high values of R_k. In order to investigate the possible effects of the interaction terms $\Delta_{k,m}$, the model (4.14) was run (in Cartesian coordinates) using DsTool, with parameters as in figure 9, except for $Z_2 = 0$, $\Delta_{1,1} = \Delta_{1,2} = \Delta_{2,2} = 0$ and $\Delta_{2,1} = -5$. A periodic orbit, period doublings and chaotic behaviour were found. The mechanism for the chaotic behaviour is similar to the two-mode mechanism in the previous subsection, when two modes are excited externally: both modes influence each others eigenfrequency, hence causing continuous regime changes towards the bent resonance curves. The difference is that the second mode is internally excited by the first one. The external tide ζ_e is a single sinusoid.

The previous paragraph considered the influence of new interaction terms in the amplitude equations due to Coriolis effects. Another possible source of additional terms is if the non-resonance conditions (3.12*d*) for the derivation of the Landau equation are violated. In fact, the intermediate equation (3.27) shows the nonlinear terms in the amplitude equations without assuming the absence of third-order resonances. Many of those terms also allow for the possibility of one mode exciting (or rather destabilizing) another. Although the non-resonance conditions (3.12*d*) are fulfilled generically, there may be symmetrical situations causing some internal resonances between eigenmodes to occur. For a rectangular basin the eigenfrequencies are $\omega_j = (j + \frac{1}{2})\sqrt{\gamma}\pi$ (§ 3.4), whence second-order resonances are clearly absent, but $\omega_k = \omega_l + \omega_m - \omega_n$ holds whenever $k = l + m - n$. The resulting extra terms in the amplitude equations may also lead to complicated behaviour in the presence of only one harmonic component in the external tidal forcing.

Several mechanisms leading to chaotic behaviour in co-oscillating tidal basins have been discussed in this and in the previous subsection. It will not always occur in all real basins, but can be found under several types of specific conditions on the external forcing and the geometry of the basin. A mathematically rigorous proof of the existence of chaotic dynamics has been elaborated for the first case (two components in near resonance with a single mode) only, although there are clear indications that it occurs in many more situations. We conclude this section with the observation that there are several mechanisms that could in principle lead to chaotic tidal dynamics.

5. Conclusions and discussion

In this paper a weakly nonlinear analysis was performed on the two-dimensional depth-averaged shallow-water equations (2.1), (2.2) in a basin co-oscillating with an adjacent sea. In that respect the scope is fairly general; except for assuming the aspect ratio (depth over width) to be small enough to ignore vertical differences, no additional assumptions on the shape of the basin are required for using (2.1). This system is investigated in the limit of small amplitudes (compared to the depth of the basin) and strong resonance (amplitude in basin much larger than at sea, i.e. for forcing frequency close to one of the eigenfrequencies and weak friction). In this limit, the behaviour of the system is dominated by its linear eigenmodes to first order. They are found from first-order (linearized) theory, with constant but

https://doi.org/10.1017/S0022112004001223 Published online by Cambridge University Press

unknown amplitudes. Nonlinear interactions between eigenmodes occur at higher order, causing the amplitudes of the eigenmodes to vary slowly in time. The ultimate result of the weakly nonlinear analysis is the Landau equation (3.28) describing the (slow) evolution of the amplitudes.

Truncation of the nonlinear dynamical system (3.28), which describes the behaviour of all amplitudes, to a finite number of modes is natural, see §4.1. Truncating to a single mode, one finds that the effective eigenfrequency of the eigenmode is changed with increasing amplitude. This causes bending of the response curve, the response amplitude as a function of forcing frequency, leading to multiple equilibria: under the same external conditions the basin can be in either a high- or low-amplitude regime, depending on the history of the sea state within the basin. Sudden regime changes may occur under slight changes of the external conditions. Moreover, if the forcing tide at sea is quasi-periodic, i.e. consisting of multiple constituents such as the lunar M_2 and solar S_2 components, chaotic behaviour of regime changes is possible. Truncating at two modes, interactions between modes come into play. The response is not a simple superposition of the results for one mode. Interaction between modes alters the region in parameter space for which resonance occurs; it leads to Hopf bifurcations, periodic orbits and chaos.

Several mechanisms leading to chaos under different circumstances were described in §4.4. Moreover, many other nonlinear processes lead to the same amplitude equations: the truncation of (3.28) to one mode leads to (4.3) and (4.4), which are the same equations as those found by Maas (1997), Maas & Doelman (2002) and Doelman *et al.* (2002) for the amplitude of the Helmholtz mode in an almost-enclosed basin, where the nonlinearity results from non-uniform hypsometry, i.e. an increase of the wet area with rising tide as is the case for a sloping bottom and tidal flat systems. The nonlinear effect due to the change in cross-sectional area of the inlet channel as a function of the water level, described in Miles (1981), leads to similar results. Actually, a change in cross-sectional area of the inlet channel is equivalent to a hypsometry change. Both cause a nonlinear relationship between the current through the channel and the resulting water-level change in the basin. In summary, advection and continuity (which are the nonlinear processes in the shallow-water equations (2.1)), changing cross-section of the inlet channel (Miles 1981) and non-uniform hypsometry (Doelman *et al.* 2002) all lead to similar results. The fact that many nonlinear processes lead to the same description suggests that (3.28) is a universal equation whose coefficients $\Gamma_{k,m}$ are determined by many contributions, possibly including ones that have not yet been identified.

Although the terminology used in this paper and the scaling assumptions following (3.1) are appropriate for basins with megatides in particular, the analysis performed in this paper may be relevant for secondary undulations as well. In that case the primary tidal oscillation period is much longer than that of the basin's eigenmodes. The latter determine the time scale of the model (3.2), (3.3) so the tidal oscillation amounts to a slow change of the reference water depth $D^{(0)}$. Hence the eigenmodes of the basin change on the tidal time scale. If the tidal time scale corresponds to the slow time scale $\tau = \alpha^2 t$, this change must be incorporated in the amplitude equations. Under the same assumptions (3.12) on the eigenmodes as before, this would lead to a parametric forcing term in the Landau equation (3.28). For the Helmholtz mode in an almost-enclosed basin this case was explored more explicitly by Maas & Doelman (2002, §5). Although similar in principle, the technical details become much more involved for the more general approach in this paper.

https://doi.org/10.1017/S0022112004001223 Published online by Cambridge University Press

Because the focus of this paper is on the interaction of the oscillatory modes with themselves, the zero-mode has been omitted (see the first Remark at the end of § 3.1). Technical aspects are more involved for the zero-mode because it cannot be described with a single amplitude. Pratt & Llewellyn Smith (1997) provide a method to deal with the latter aspect, but the incorporation of both the zero- and oscillatory modes into a consistent theory for small amplitudes still forms a mathematical challenge that remains to be solved. However, the effect of the zero-mode on the oscillatory modes is expected to cause some interesting behaviour. Just like the Earth's rotation and non-trivial third-order resonances, it may trigger internal excitation of modes that are not excited by the tide at sea directly. The presence of multiple modes with non-zero amplitude can lead to chaotic behaviour through their interaction described in this paper, see § 4.

In view of the assumptions in this paper, one might wonder about the geophysical relevance of the amplitude equation (3.28). The parameter $\alpha = Z/H$ measures the importance of the nonlinear terms in (3.2). Moreover, it has been used as a scaling parameter to reflect the assumptions of strong resonance, so α also appears in the amplification factor, frequency detuning and bottom friction. The slow time scale τ on which the amplitudes evolve is $O(\alpha^{-2})$, typically some tens of periods (note that time was scaled with the eigenperiod T and a factor of 2π according to (3.1)), i.e. tens of days for tidal systems and one or two days in the case of secondary undulations. The results in this paper suggest that the dynamics can be chaotic if modulation of the exterior tide occurs at the same time scale, due to e.g. the spring-neap tidal cycle (14 day period) in the tidal case or the basic (semi)diurnal tide in the case of secondary undulations.

The assumption of strong resonance may seem to be in contradiction with the assumption of small amplitudes. In reality however, tidal motion usually is small compared to the total water depth. Moreover, tides at sea are smaller than those in the basin due to amplification by resonance. The assumptions in this work pertain to this limit of the observations. The main reason for the assumption of small detuning and large amplification is to maintain analytical tractability. The nonlinear effects will be equally important as long as the tidal amplitude in the basin remains large enough. Physically the important processes are friction and nonlinearity. The nonlinear effects change the effective eigenfrequency as a function of the tidal amplitude in the basin, i.e. of α, hence bending the resonance curve. Apart from the fact that friction reduces the tidal amplitude, it tends to smooth the response curve and thereby hides the nonlinear effects. Still, if α, hence the nonlinear effects, is less small, friction may not need to be that small either. Although the validity of the results of the weakly nonlinear analysis may be confined to this limit, it is quite possible that the processes described here do play a role beyond the small-amplitude limit. After all, dependence of the effective eigenfrequency on amplitude, multiple equilibria and other nonlinear effects are generally enhanced for increasing amplitude. No analytical methods are available yet to substantiate this however.

In order to quantify the balance between friction and the nonlinear effects, one needs to consider a single equation in which both nonlinear advection and the nonlinear continuity term can be compared with friction. The main effect of the nonlinear terms considered in this paper is to change the effective eigenfrequency. This introduces phase differences between the tide in the basin and at sea. Consequently it changes the absorption of energy from the exterior tide. In line with the analysis in this paper the local energy equation can be obtained by forming the 'inner product'

https://doi.org/10.1017/S0022112004001223 Published online by Cambridge University Press

	formula	estimate	Bay of Fundy	Gulf of Nicoya	Moldefjord
a. length (km)		L	270	40	10
b. depth (m)		H	70	20	30
c. elevation (m)		Z	6	1	0.1
d. velocity (m s^{-1})		U	1	0.2	0.1
e. time scale (10^3 s)		$\frac{T}{2\pi}$	7.1	7.1	0.46
A. elevation ($m^3 s^{-3}$)	$g\zeta\frac{\partial\zeta}{\partial t}$	$2\pi\frac{gZ^2}{T}$	$5.0\cdot10^{-2}$	$1.4\cdot10^{-3}$	$2.1\cdot10^{-4}$
B. lin. cont. ($m^3 s^{-3}$)	$g\zeta\nabla\cdot(H\boldsymbol{U})$	$\frac{gHZU}{L}$	$1.5\cdot10^{-2}$	$9.8\cdot10^{-4}$	$2.9\cdot10^{-4}$
C. nl. cont. ($m^3 s^{-3}$)	$g\zeta\nabla\cdot(\zeta\boldsymbol{U})$	$\frac{gZ^2U}{L}$	$1.3\cdot10^{-3}$	$4.9\cdot10^{-5}$	$9.8\cdot10^{-7}$
D. inertia ($m^3 s^{-3}$)	$D\boldsymbol{U}\cdot\frac{\partial\boldsymbol{U}}{\partial t}$	$2\pi\frac{HU^2}{T}$	$9.8\cdot10^{-3}$	$1.1\cdot10^{-4}$	$6.5\cdot10^{-4}$
E. advection ($m^3 s^{-3}$)	$D\boldsymbol{U}\cdot([\boldsymbol{U}\cdot\nabla]\boldsymbol{U})$	$\frac{HU^3}{L}$	$2.6\cdot10^{-4}$	$4.0\cdot10^{-6}$	$3.0\cdot10^{-6}$
F. gradient ($m^3 s^{-3}$)	$gD\boldsymbol{U}\cdot\nabla\zeta$	$\frac{gHZU}{L}$	$1.5\cdot10^{-2}$	$9.8\cdot10^{-4}$	$2.9\cdot10^{-4}$
G. friction ($m^3 s^{-3}$)	$D\boldsymbol{U}\cdot\frac{\tau_b}{\rho D}$	$c_D U^3$	$2.5\cdot10^{-3}$	$2.0\cdot10^{-5}$	$2.5\cdot10^{-6}$

TABLE 2. Estimates for the order of magnitudes of the terms in the local energy equation corresponding to (2.1*b*). Summing the terms A–G and integrating over the basin area leads to the global energy. Rough quantitative scaling estimates for a couple of example basins, that were studied by Doodson (1924), Gutiérrez *et al.* (1981) and Golmen *et al.* (1994) respectively. Numbers have been taken from `http://www.town.stgeorge.nb.ca/bay.html`, `http://www.bayoffundy.com/tidetables`, Godin & Gutiérrez (1986) for the Bay of Fundy, `http://data.ecology.su.se/mnode/CentralAmerica/GulfofNicoya/nicoyabud.htm`, `http://ilikai.soest.hawaii.edu/uhslc/htmld/d0396A.html` for the Gulf of Nicoya and Golmen *et al.* (1994) for the Moldefjord.

$g\zeta$ (2.1*a*) + $D\boldsymbol{U}\cdot$(2.1*b*):

$$\underset{\text{A}}{g\zeta\frac{\partial\zeta}{\partial t}}+\underset{\text{B}}{g\zeta\nabla\cdot(H\boldsymbol{U})}+\underset{\text{C}}{g\zeta\nabla\cdot(\zeta\boldsymbol{U})}+\underset{\text{D}}{D\boldsymbol{U}\cdot\frac{\partial\boldsymbol{U}}{\partial t}}+\underset{\text{E}}{D\boldsymbol{U}\cdot([\boldsymbol{U}\cdot\nabla]\boldsymbol{U})}+\underset{\text{F}}{gD\boldsymbol{U}\cdot\nabla\zeta}+\underset{\text{G}}{D\boldsymbol{U}\cdot\frac{\tau_b}{\rho D}}=0. \tag{5.1}$$

The terms in this equation are listed in table 2 together with order of magnitude estimates based on the scales introduced in (3.1). By considering the dominant balance in the continuity equation between elevation change (A) and the linear continuity term (B), one obtains the easily interpretable relationship $UHT=2\pi LZ$, which allows us to write $\alpha=Z/H$ for the ratio between the nonlinear terms (C and E) and the time derivative (A resp. D) in both the continuity and momentum equation. The balance between inertia (D) and the pressure gradient (F) holds if the length scale L is comparable to the wavelength $\lambda=(gH)^{1/2}T$. The balance between friction (G) and advection (E) requires $c_D\sim H/L$. Because resonant basins are considered, the length of the basin L is related to H through the dispersion relation $L=\varepsilon\lambda$, where $\varepsilon=1/4, 3/4, \ldots$ for a half-open rectangular channel, cf. (3.31), whereas $\varepsilon\ll1$ for an almost-enclosed Helmholtz resonator. Consequently the balance $\varepsilon c_D\sim H/\lambda=(H/g)^{1/2}/T$ appears to hold for reasonable depth only in the case of an almost-enclosed basin. However, comparing the nonlinear continuity term (C) with friction (G), one finds analogously $\varepsilon^3 c_D\sim H/\lambda$ according to which the balance does hold for $\varepsilon=1/4$ and $H\sim10$–100 m.

https://doi.org/10.1017/S0022112004001223 Published online by Cambridge University Press

Quantitative estimates of the respective scales are given in table 2 for a couple of example basins to which the presented model might be applicable. In view of the observation that many different processes lead to the same amplitude equations (3.28), its relevance may be broader, with many processes contributing to $\Gamma_{k,m}$. When the effective eigenfrequency depends on the amplitude of the motion, (3.28) describes the first-order evolution of the amplitudes on a longer time scale, possibly leading to chaotic behaviour. Obviously, identifying such qualitative effects of nonlinearity in time series of observed tidal amplitudes would be the best proof of the relevance of (3.28).

Predictions of tides are often based on tidal harmonics, the amplitudes and phases of which are constant in linear theory, describing the tidal signal as a superposition of harmonic components. In many cases this works quite well, but there are clearly deviations. They are usually attributed to meteorological disturbances. The observational challenge is to distinguish between meteorological effects and internally induced deviations (Vittori 1992). Some first steps using an approach apt for chaotic systems have been made in Frison *et al.* (1999). They state that the tidal signal becomes increasingly irregular when progressing into complicated basins. This is consistent with our findings, attributing chaotic behaviour to nonlinear resonance phenomena. However, note that their work is on the time series of *in situ* water levels themselves, whereas in this paper the amplitudes of eigenmodes are considered. More specifically, we suggest considering the time series describing the evolution of harmonic constants, as was done on a year to year time scale by Doodson (1924). He identified three perturbations on the harmonic constants for St. John, Bay of Fundy and Bombay, two of which he found to be related to astronomical forcing and one of which remained unaccounted for. More recently Gutiérrez *et al.* (1981) studied fluctuations of the harmonic constants for Puntarenas (situated at the Gulf of Nicoya, Pacific coast of Costa Rica) and Trieste (North Adriatic Sea) and found that they do not result from non-perfect selectivity of the analysis. They condensed the variation into a single value for its variance however; we have no knowledge of studies in which time series of harmonic constants have been tested for chaotic dynamics. We hope that our findings may spur further data investigation of this kind, both on tidal records (on a fortnightly time scale) and on secondary undulations (on a daily time scale). Because the latter are relatively unimportant for the water level, they have been investigated less extensively until recently, but their influence on currents can be considerable and irregular behaviour of secondary undulations had already been reported at the beginning of the twentieth century, see Honda *et al.* (1908) and Nakano (1932). Clear evidence of nonlinearity would be the occurrence of sudden regime changes and hysteresis: the response of the basin depending on its history, disturbances having lasting effects after the decay of transient behaviour. Sudden changes of the tidal regime in the past may be detected from their geological signature (Oost 1995).

Apart from reinvestigating time series of observed water levels, the nonlinear mechanisms can also be studied by means of laboratory experiments. Elaborating on the work by Maas (1997) on the nonlinear effects due to non-uniform hypsometry in an almost-enclosed basin, a laboratory tank has been created to simulate a Helmholtz resonator. Publications on the results of experiments performed with this tank are in preparation. Nonlinear effects bending the response curves have been found and multiple equilibria were observed, although other processes than the hypsometry also play an important role in causing this.

https://doi.org/10.1017/S0022112004001223 Published online by Cambridge University Press

The authors thank Huib de Swart for carefully reading and commenting the manuscript and Tom Koornwinder and Peter Stevenhagen for their help in validating the nonresonance conditions in § 3.4.

Appendix. Excluding nontrivial resonances for the examples in § 3.4.

In this Appendix it is shown that the estimate (3.34) implies that there are no nontrivial resonances for which $\varpi_k - \varpi_l - \varpi_m + \varpi_n = 0$. First of all, direct application of the estimate leads to

$$\begin{aligned}\varpi_k - \varpi_l - \varpi_m + \varpi_n &= a(k-l-m+n) - \frac{1}{4k-1} + \frac{1}{4l-1} + \frac{1}{4m-1} - \frac{1}{4n-1} \\ &\quad + \frac{\chi_k}{(4k-1)^3} - \frac{\chi_l}{(4l-1)^3} - \frac{\chi_m}{(4m-1)^3} + \frac{\chi_n}{(4n-1)^3} \\ &= a(k-l-m+n+\varepsilon)\end{aligned}$$

with $-1 < \varepsilon < 1$. This does not rule out resonances of this kind, but it does show that one must have $\varepsilon = 0$ and $k + n = l + m$ for these resonances to occur. Because $0 < \chi_j < \bar{\chi}$, with $\bar{\chi} = 31/(3\pi^2)$ for the linear, or $\bar{\chi} = \frac{27}{128}\sqrt{2}$ for the quadratic bottom, we can estimate

$$\left| \frac{\chi_k}{(4k-1)^3} - \frac{\chi_l}{(4l-1)^3} - \frac{\chi_m}{(4m-1)^3} + \frac{\chi_n}{(4n-1)^3} \right| < \frac{2\bar{\chi}}{(4n-1)^3},$$

for $k > l \geqslant m \geqslant n \geqslant 1$. Next, we introduce

$$\chi = (4n-1)^3 \left(\frac{1}{4k-1} - \frac{1}{4l-1} - \frac{1}{4m-1} + \frac{1}{4n-1} \right). \tag{A 1}$$

If it can be shown that $\chi > 2\bar{\chi}$ if $k > l \geqslant m \geqslant n \geqslant 1$ and $k + n = l + m$, the possibility that $\varpi_k - \varpi_l - \varpi_m + \varpi_n = 0$ is ruled out. We will show that $\chi \geqslant \frac{288}{77}$. In fact, $\frac{288}{77} > 2\bar{\chi}$ both for the linear and for the quadratic bottom.

In order to prove that $\chi \geqslant \frac{288}{77}$, factor (A 1) into

$$\chi = 2^5 \frac{(4n-1)^2(2s-1)(lm-kn)}{(4k-1)(16lm-4s+1)}$$

writing $s = k + n = l + m$. As a function of lm for fixed k, n (and s), this is minimized for minimal lm, hence for $l = k-1$, $m = n+1$ (note that $k > l$ implies $m > n$ because $k + n = l + m$). Therefore

$$\chi \geqslant 2^5 \frac{(4n-1)^2(2s-1)}{(4k-1)} \frac{(k-1)(n+1)-kn}{(16(k-1)(n+1)-4s+1)} = 2^5 \frac{(4n-1)^2(s-2n-1)(2s-1)}{(4n+3)(4k-1)(4k-5)},$$

which is minimal with respect to n, k for $n = 1$, $k = s-1$, so $\chi \geqslant 2^5 \frac{9}{7} \frac{(2s-1)(s-3)}{(4s-5)(4s-9)}$. For $s \geqslant 4$ (which follows from the fact that $s > k > l \geqslant m > n \geqslant 1$) this is minimized at $s = 4$, so finally the estimate $\chi \geqslant \frac{288}{77}$ is reached.

REFERENCES

Candela, J., Mazzola, S., Sammari, C., Limeburner, R., Lozano, C. J., Patti, B. & Bonnano, A. 1999 The "mad sea" phenomenon in the Strait of Sicily. *J. Phys. Oceanogr.* **29**, 2210–2231.

Defant, A. 1961 *Physical Oceanography*, vol. 2. Pergamon.

https://doi.org/10.1017/S0022112004001223 Published online by Cambridge University Press

Doelman, A., Koenderink, A. F. & Maas, L. R. M. 2002 Quasi-periodically forced nonlinear Helmholtz oscillators. *Physica* D **164**, 1–27.

Doodson, A. T. 1924 Perturbations on harmonic constants. *Proc. R. Soc. Lond.* A **106**, 513–526.

Dronkers, J. J. 1962 The linearization of the quadratic resistance term in the equation of motion for a pure harmonic tide in a sea. In *Proc. Symp. on Mathematical-Hydrodynamical Methods in Physical Oceanography, Hamburg*.

Dronkers, J. J. 1964 *Tidal Computations in Rivers and Coastal Waters*. North-Holland.

Fabrikant, A. L. 1995 Harbour oscillations generated by shear flow. *J. Fluid Mech.* **282**, 203–217.

Flemming, B. W. & Bartholomä, A. (Eds.) 1995 *Tidal Signatures in Modern and Ancient Sediments*, *Special Publication* 24, International Association of Sedimentologists. Blackwell Science.

Frison, T. W., Abarbanel, H. D. I., Earle, M. D., Schultz, J. R. & Scherer, W. 1999 Chaos and predictability in ocean water levels. *J. Geophys. Res.* **104**, 7935–7951.

Garrett, C. 1975 Tides in gulfs. *Deep-Sea Res.* **22**, 23–35.

Gatteschi, L. & Giordano, C. 2000 Error bounds for McMahon's asymptotic approximations of the zeros of the Bessel functions. *Integral Transform. Spec. Funct.* **10**, 41–56.

Giese, G. S. & Chapman, D. C. 1990 Coastal seiches. *Oceanus* **36**, 38–46.

Godin, G. & Gutiérrez, G. 1986 Nonlinear effects in the tide of the Bay of Fundy. *Cont. Shelf Res* **5**, 379–402.

Golmen, L. G., Molvaer, J. & Magnusson, J. 1994 Sea level oscillations with super-tidal frequencies in a coastal embayment of western Norway. *Cont. Shelf Res.* **14**, 1439–1454.

Gomis, D., Monserrat, S. & Tintoré, J. 1993 Pressure-forced seiches of large amplitude in inlets of the Balearic Islands. *J. Geophys. Res.* **98**, 14437–14445.

Green, T. 1992 Liquid oscillations in a basin with varying surface area. *Phys. Fluids* A **4**, 630–632.

Guckenheimer, J. M., Back, A., Myers, M., Wicklin, F. & Worfolk, P. 1992 DsTool: Computer assisted exploration of dynamical systems. *Not. Am. Math. Soc.* **39**, 303–309.

Guckenheimer, J. M. & Holmes, P. J. 1983 *Nonlinear Oscillations, Dynamical Systems, and Bifurcations of Vector Fields*. Springer.

Gutiérrez, A., Mosetti, F. & Purga, N. 1981 On the indetermination of the tidal harmonic constants. *Nuovo Cimento* **4**, 563–575.

Hibiya, T. & Kajiura, K. 1982 Origin of the *Abiki* phenomenon (a kind of seiche) in Nagasaki Bay. *J. Oceanogr. Soc. Japan* **38**, 172–182.

Honda, K., Terada, T., Yoshida, Y. & Isitani, D. 1908 Secondary undulations of oceanic tides. *J. Coll. Sci. Imp. Univ. Tokyo* **24**, 1–113 and 95 plates.

Kabbaj, A. & Le Provost, C. 1980 Nonlinear tidal waves in channels: a perturbation method adapted to the importance of quadratic bottom friction. *Tellus* **32**, 143–163.

Krauss, W. 1973 *Methods and Results of Theoretical Oceanography*, vol. I: Dynamics of the homogeneous and the quasihomogeneous ocean. Berlin-Stuttgart: Gebrüder Borntraeger.

LeBlond, P. H. & Mysak, L. A. 1978 *Waves in the Ocean*. Elsevier.

Le Provost, C. 1973 Décomposition spectrale du terme quadratique de frottement dans les équations des marées littorales. *C.R. Acad. Sci. Paris* **276**, 571–574, 653–656.

Lorentz, H. A. 1922 Het in rekening brengen van den weerstand bij schommelende vloeistofbewegingen. *De Ingenieur* p. 695.

Maas, L. R. M. 1997 On the nonlinear Helmholtz response of almost-enclosed tidal basins with sloping bottoms. *J. Fluid Mech.* **349**, 361–380.

Maas, L. R. M. & Doelman, A. 2002 Chaotic tides. *J. Phys. Oceanogr.* **32**, 870–890.

Mei, C. C. 1989 *The Applied Dynamics of Ocean Surface Waves*. World Scientific.

Miles, J. W. 1971 Resonant response of harbors: an equivalent-circuit analysis. *J. Fluid Mech.* **46**, 241–265.

Miles, J. W. 1981 Nonlinear Helmholtz oscillations in harbours and coupled basins. *J. Fluid Mech.* **104**, 407–418.

Munk, W. H. & Cartwright, D. E. 1966 Tidal spectroscopy and prediction. *Phil. Trans. R. Soc. Lond.* **259**, 533–581.

Nakano, M. 1932 Preliminary note on the accumulation and dissipation of energy of the secondary undulations in a bay. *Proc. Phys.-Math. Soc. Japan* **14**, 44–56.

Nayfeh, A. H. & Mook, D. T. 1979 *Nonlinear Oscillations*. *Pure and Applied Mathematics*. John Wiley & Sons.

https://doi.org/10.1017/S0022112004001223 Published online by Cambridge University Press

Nycander, J. & Döös, K. 2001 Open boundary conditions for barotropic waves. *Sci. Rep.* FOI-R–0078–SE. FOI — Swedish Defence Research Agency, Systems Technology, SE-172 90 Stockholm, ISSN 1650-1942.

Okihiro, M. & Guza, R. T. 1995 Infragravity energy modulation by tides. *J. Geophys. Res.* **100**, 16143–16148.

Oost, A. P. 1995 Sedimentological implications of morphodynamic changes in the ebb-tidal delta, the inlet and the drainage basin of the Zoutkamperlaag tidal inlet (Dutch Wadden Sea), induced by a sudden decrease in the tidal prism. In *Tidal Signatures in Modern and Ancient Sediments* (ed. B. W. Flemming & A. Bartholomä), pp. 101–119. Blackwell.

Parker, B. B. 1991 The relative importance of the various nonlinear mechanisms in a wide range of tidal interactions(review). In *Tidal Hydrodynamics* (ed. B. B. Parker), pp. 237–268. John Wiley & Sons.

Pratt, L. J. 1997 Hydraulically drained flows in rotating basins. part II: Steady flow. *J. Phys. Oceanogr.* **27**, 2522–2535.

Pratt, L. J. & Llewellyn Smith, S. G. 1997 Hydraulically drained flows in rotating basins. part I: Method. *J. Phys. Oceanogr.* **27**, 2509–2521.

Vittori, G. 1992 On the chaotic structure of tide elevation in the Lagoon of Venice. In *Proc. 23rd Intl Conf. on Coastal Engineering, Venice* (ed. B. L. Edge), pp. 1826–1839. ASCE.

Wiggins, S. 1988 *Global Bifurcations and Chaos*. Springer.

Zimmerman, J. T. F. 1992 On the Lorentz-linearization of a nonlinearly damped tidal Helmholtz oscillator. *Proc. Kon. Ned. Akad. v Wet.* **95** (1), 127–145.

https://doi.org/10.1017/S0022112004001223 Published online by Cambridge University Press